

Boise State University

ScholarWorks

Geosciences Faculty Publications and
Presentations

Department of Geosciences

4-1-2023

Tectonomagmatic Evolution of Southwestern Laurentia: Insights from Zircon U-Pb Geochronology and Hafnium Isotopic Composition of the Red Bluff Granite Suite, West Texas, USA

Munazzam Ali Mahar
University of Texas at El Paso

Philip C. Goodell
University of Texas at El Paso

Jason W. Ricketts
University of Texas at El Paso

Eric J. Kappus
Southwest University at El Paso

James L. Crowley
Boise State University

See next page for additional authors

Authors

Munazzam Ali Mahar, Philip C. Goodell, Jason W. Ricketts, Eric J. Kappus, James L. Crowley, and Anthony M. Alvarez



Tectonomagmatic evolution of southwestern Laurentia: Insights from zircon U-Pb geochronology and hafnium isotopic composition of the Red Bluff Granite Suite, west Texas, USA

Munazzam Ali Mahar¹, Philip C. Goodell¹, Jason W. Ricketts¹, Eric J. Kappus², James L. Crowley³, and Anthony M. Alvarez¹

¹Department of Earth, Environmental and Resource Sciences, The University of Texas at El Paso, El Paso, Texas 79968, USA

²Southwest University at El Paso, El Paso, Texas 79925, USA

³Department of Geosciences, Boise State University, Boise, Idaho 83725, USA

ABSTRACT

We provide laser ablation–multicollector–inductively coupled plasma–mass spectrometry (LA-MC-ICP-MS) and high-precision chemical abrasion–isotope dilution–thermal ionization mass spectrometry (CA-ID-TIMS) U-Pb ages and Hf isotopic compositions of zircons from the Red Bluff Granite Suite and mafic dikes in the Franklin Mountains of El Paso, Texas, USA. Granitoids exposed in the Franklin Mountains were previously divided into five magmatic stages based on cross-cutting relationships. Major and trace element compositions showed that these granitoids are ferroan, alkaline, and A2 type. Homogeneity in the whole-rock geochemistry suggests that the granite stages are genetically related and share similar petrogenetic histories. Weighted mean zircon ²⁰⁶Pb/²³⁸U dates from the older magmatic stage 1 alkali-feldspar quartz syenite and stage 2 alkali-feldspar granite are 1112.36 ± 0.35 and 1112.46 ± 0.37 Ma, respectively. The weighted mean εHf(t) values varying from +5.3 to +7.2 are similar to those of other regional ca. 1.1 Ga magmatic rocks throughout southwestern Laurentia. Geochemical characteristics, petrological modeling, and enriched Hf isotopic composition suggest fractional crystallization of a basaltic magma that was produced by melting of an enriched mantle reservoir. However, zircon inheritance ages of ca. 1.3 Ga and 1.26–1.15 Ga are consistent with a minor contribution from felsic crustal basement. Our data and regional geology are consistent with a post-collisional slab break-off that facilitated asthenospheric upwelling and partial melting of the enriched mantle, possibly subcontinental lithospheric mantle, extending from Llano Uplift, Texas, in the southeast to California to the northwest. Magma thus generated upon differentiation produced ferroan and A-type granitoids.

INTRODUCTION

The ferroan and alkaline Red Bluff Granite Suite (RBGS) in the Franklin Mountains of west Texas, USA (Fig. 1), offers an opportunity for understanding

munazzam ali mahar <https://orcid.org/0000-0002-2590-3041>

the late Mesoproterozoic tectonomagmatic evolution of the southwestern Laurentian convergent margin. Previously, on the basis of geochemical data from granitic rocks and basaltic dikes, Shannon et al. (1997) suggested that the ca. 1.1 Ga granitic magma was produced through fractional crystallization of a ferrobasaltic magma. Norman et al. (1987), Smith et al. (1997), and Barnes et al. (1999) proposed that juvenile crustal material was either directly derived from the subcontinental lithospheric mantle or recently emplaced basaltic underplate with minimal input from evolved crustal sources. The low ⁸⁷Sr/⁸⁶Sr (–0.7034; Norman et al., 1987) and positive εNd (+2.5 to +3.8; Norman et al., 1987; Patchett and Ruiz, 1989) coupled with primitive initial Pb isotopic compositions suggest fractionation of a basaltic parent (Smith et al., 1997).

Tectonically, magmatism in west Texas (i.e., El Paso region) has been variably interpreted as produced in a subduction zone (e.g., Norman et al., 1987; Roths, 1993) or anorogenic intracontinental rift (e.g., Norman et al., 1987; Keller et al., 1989; Adams and Keller, 1994; Kargi and Barnes, 1995; Shannon et al., 1997; Bickford et al., 2000). Recently, Davis and Mosher (2015) interpreted the Proterozoic tectonic configuration of central and west Texas based primarily on the geologic and structural record preserved in the Llano Uplift and Van Horn areas. The Llano Uplift is located 250 km south-southeast of the Grenville Front (i.e., Llano Front of west Texas; Mosher, 1993) whereas the Van Horn area lies within the Llano Front (Fig. 1). The Llano Front is part of the Grenville Front, which is interpreted as a possible tectonic extent of Grenville deformation separating deformed metamorphic rocks to the south from the undeformed granites and rhyolites belonging to the 1.4–1.3 Ga Southern Granite-Rhyolite province (Van Schmus et al., 1996). The Llano Front is defined by gravity data and Nd model ages (Ewing, 1990; Mosher, 1993; Bickford et al., 2000). Mosher (1998) suggested that the deformed 1.4–1.3 Ga metasedimentary and metavolcanic rocks thrust over 1.25 Ga siliciclastic and volcanic rocks (Soegaard and Callahan, 1994) in the Van Horn region are the manifestation of the continuation of the Llano Front in the Van Horn region. However, undeformed RBGS and carbonate and volcanic rocks in El Paso are located further to the northwest of the Llano Front.

On the basis of the geological and structural evolution of the Van Horn and Llano areas, Mosher (1998) and Mosher et al. (2008) proposed slab break-off

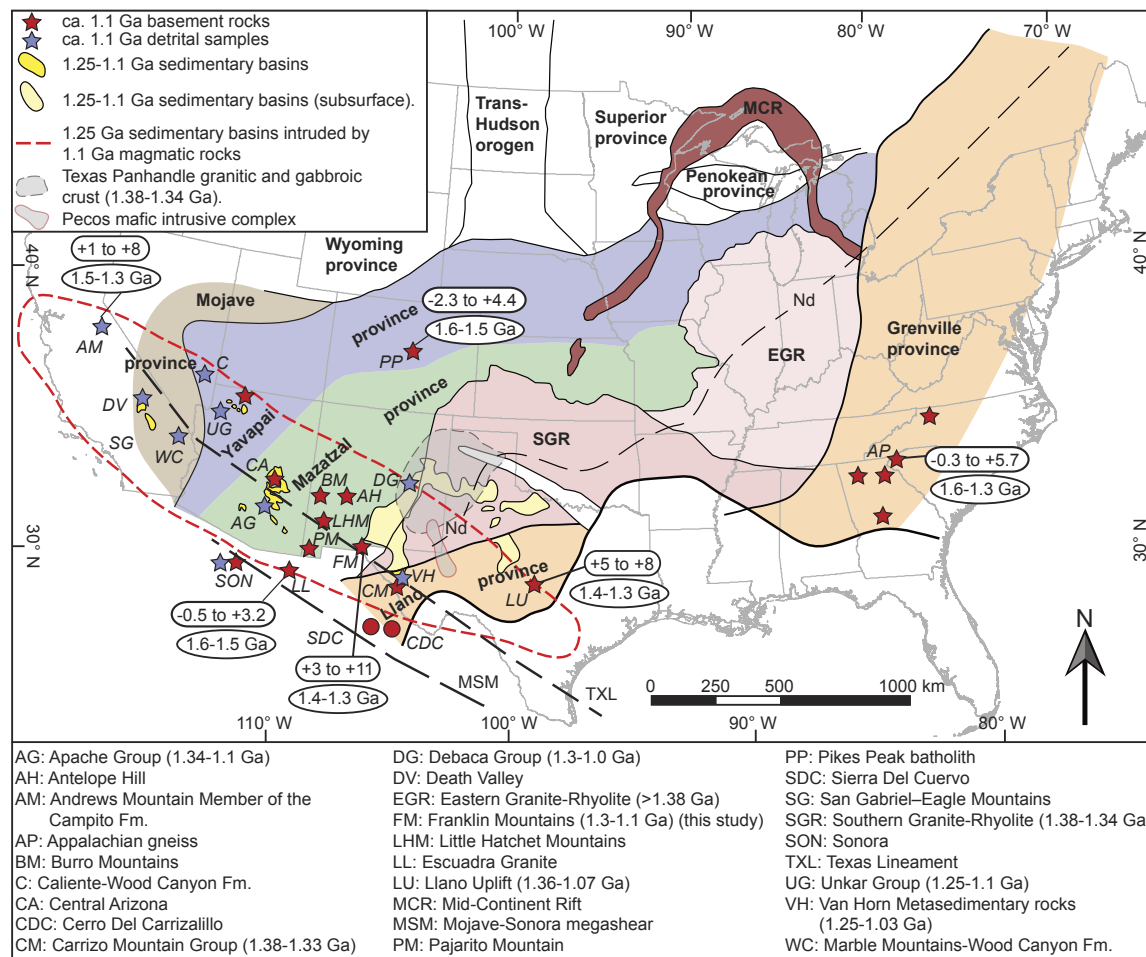


Figure 1. Map showing Precambrian basement provinces of United States (modified from Bickford et al., 2015) as well as pre-Neoproterozoic basement terranes, sedimentary basins, structural features, and magmatic rocks (after Timmons et al., 2005; Howard, 2013; Bright et al., 2014; Mulder et al., 2017). Nd line represents boundary which separates granites and rhyolites of cratonal origin to the northwest (Nd model ages = 1.8–1.6 Ga) from the juvenile origin to the southeast (Nd model ages = 1.5–1.4 Ga; Bickford et al., 2015, and references therein). Initial hafnium isotopic compositions [eHf(t)] and hafnium depleted mantle model ages (Hf T_{DM}) (shown in white ovals) for 1.1 Ga basement rocks and detrital zircons are calculated from data presented in Howard (2013) and this study.

during post-orogenic extension. Davis and Mosher (2015) suggested an initial northward movement of a southern continent relative to Laurentia, which resulted in northeastward tectonic transport for central Texas in the Llano region. They postulated that the ca. 1.15–1.12 Ga magmatism, metamorphism, and deformation in the Llano Uplift is the manifestation of indentation of the northeastern edge of a southern continent into Laurentia. Deformation observed in Van Horn region is attributed to a 60 m.y. clockwise rotation of this southern continent and prolonged subduction, which culminated in continent-continent collision at ca. 1.06–0.98 Ga.

Such a model may explain the post-collision (ca. 1.09–1.07 Ga; Walker, 1992; Helper, 1996; Rougvie et al., 1999) magmatism and deformation observed in

the Llano and Van Horn areas but is unable to explain the 1.1 Ga origin of the RBGS located 140 km further northwest of the Llano Front, the hinterland of the Laurentian subducting slab to the south. Smith et al. (1997) suggested that the contrasting geochemistry and petrology of granites from west (i.e., RBGS) and central Texas cannot be explained by a single magmatic event. A possible cause for this discrepancy is the location of the RBGS with respect to the Llano Front. Also, unlike in the Van Horn and Llano areas, rocks in the Franklin Mountains are undeformed. The undeformed RBGS was emplaced within the 1.25 Ga shelf sequences northwest of the Llano Front, suggesting that the 1.1 Ga magmatism must have been produced within Laurentia and not the southern collider. In contrast, Llano granitoids intruded the deformed and

metamorphosed Laurentian crust during syn- to post-collision slab break-off of a presumably southward-descending Laurentian slab (Davis and Mosher, 2015). Thus, these models are not intended to resolve the origin of ca. 1.1 Ga RBGS magmatism and are unable to explain the thermal perturbation further to the northwest in the Franklin Mountains at the time when the Llano Uplift was in active continent-continent collision followed by slab break-off. On the basis of previous geochemical and isotopic studies from the RBGS, Mosher (1998) invoked extension within an overall collision zone for the origin of RBGS magmatism. However, the model of Mosher (1998) does not work for the Franklin Mountains because deformation in the west Texas Van Horn region occurred from ca. 1060 to 980 Ma (Grimes and Copeland, 2004). Therefore, collision in the Llano and subsequently in the Van Horn area with a southern collider (e.g., Davis and Mosher, 2015) cannot explain rifting and emplacement of the RBGS.

In this work, we present laser ablation–multicollector–inductively coupled plasma–mass spectrometry (LA-MC-ICP-MS) and chemical abrasion–isotope dilution–thermal ionization mass spectrometry (CA-ID-TIMS) zircon U–Pb ages, zircon Hf isotopic compositions, and additional whole-rock geochemistry of granites and mafic dikes. In addition to our data from the RBGS, we used Hf isotopic data reported in Howard (2013) to calculate depleted mantle model ages for the 1.1 Ga magmatic rocks across the entire stretch of the southwestern Laurentian front. These new U–Pb dates and time-constrained Hf isotopic data from zircon from the RBGS are then integrated with the regional U–Pb ages, and Hf and Nd isotopic data to explore the genetic relationships among widespread late Mesoproterozoic magmatic rocks that intruded the carbonate and siliciclastic basin deposits from west Texas to California. This integrated approach has provided deeper insights into the timing and origin of the RBGS of west Texas in the regional Grenville tectonic framework.

■ CORRELATION OF MESOPROTEROZOIC SEDIMENTARY AND MAGMATIC ROCKS AND TECTONIC EVOLUTION OF SOUTHWESTERN LAURENTIA

Mesoproterozoic magmatism and sedimentary deposition extending from central Texas to California were synchronous with the Grenville orogeny from ca. 1255 to 980 Ma (McLelland et al., 1996; Mulder et al., 2017). The resulting deposits are of particular interest because they were intruded by 1.1 Ga magmas throughout the Laurentian Front (e.g., Shannon et al., 1997). The origin of the sedimentary deposits and associated magmatism might have resulted from the convergence of the southwestern Laurentian margin with a southern continent, possibly Kalahari (Mulder et al., 2017, and references therein). This convergent margin is suggested to have evolved from an arc-continent to a continent-continent collision zone and later recorded post-collision destabilization (break-off) of the Laurentian slab (Mosher et al., 2008; Mulder et al., 2017). Sedimentary sequences extending from the Llano region to California have been correlated based on similar lithology, timing, and environment of deposition (e.g., Wrucke, 1989; Mosher, 1998; Seeley, 1999; Bickford et al.,

2000; Timmons et al., 2005; Spencer et al., 2014). Whereas Bickford et al. (2000) provided correlations between rocks exposed in Van Horn and El Paso regions, Timmons et al. (2005) provided a correlation throughout southwestern Laurentia. Mulder et al. (2017), on the basis of detrital zircon, muscovite, and biotite ages, provided a more detailed regional correlation for late Mesoproterozoic sedimentation and its possible connection to the Grenville orogeny.

We modified the regional stratigraphic correlation to emphasize the magmatic activity during 1200–1155 Ma on the basis of previous (and from this study) geochronological data from magmatic rocks and detrital zircons; this period was missing in previous correlations (e.g., Mulder et al., 2017) (Fig. 2). Metagabbroic, metadioritic, metabasaltic, and granitic rocks in Sierra del Cuervo in northern Mexico suggest the development of a continental margin island arc (Blount, 1993; Mosher, 1998) from 1.38 to 1.34 Ga (Fig. 2). Lower Apache, Pahrump, and possibly upper Carrizo Group of west Texas, synchronous with regional magmatism, represent the earliest sediments deposited in the distal backarc basin formed along the southwestern Laurentian margin from 1.34 to 1.32 Ga. Subsequently, from 1.25 to 1.23 Ga, shallow marine carbonate, mudstone, sandstone, and siliciclastic units were deposited within the basin from Llano region in the southeast to California in the northwest. These deposits are intercalated with extrusive rocks and intruded by 1.25 and 1.1 Ga felsic and mafic rock assemblages. This is consistent with the Grenville-age detrital zircons within the Cambrian–Ordovician Bliss Sandstone in southern New Mexico with the main peak at 1250 Ma and a significant number of dates ranging from 1.1 to 1.0 Ga (Amato and Mack, 2012). The Castner Marble and Mundy Breccia package in the Franklin Mountains correlates with the Allamoore and Tumbledown Formations of the Van Horn area to the southeast and with the Debaca Group (New Mexico), the Mescal Limestone (eastern Arizona), the Bass Formation (Grand Canyon, Arizona), and the Crystal Spring Formation (Death Valley) to the north and northwest (Bickford et al., 2000; Timmons et al., 2005; Mulder et al., 2017). The Lanoria Formation correlates well with the Troy Quartzite of northern Arizona and the Dox Formation–Shinumo Sandstone of the Grand Canyon (Mulder et al., 2017). Spencer et al. (2014) correlated the Lanoria Formation with the Hazel Formation in the Van Horn area based on detrital zircon dates. Mulder et al. (2017) suggested that during 1.25–1.23 Ga a southward-located slab was subducting underneath Laurentia, resulting in the formation of a retroarc basin above the Laurentian basement (upper plate); sediments were derived partly from the active continental arc along the southern margin of Laurentia. In contrast, Bickford et al. (2000) proposed deposition of these sedimentary sequences within rift basins on the basis of the shallow-water depositional environment of the Allamoore Formation, low-grade metamorphic rocks of west Texas, and bimodal volcanism.

Finally, felsic magmatic rocks as well as sedimentary sequences were intruded by basaltic magmas from 1.1 to 0.9 Ga (e.g., Bright et al., 2014). Basaltic dikes within the RBGS were correlated with those found in the Allamoore Formation of the Van Horn region, Texas (e.g., Norman et al., 1987). Similar basaltic dikes can be traced throughout the southwestern United States (Hammond, 1990; Howard, 1991; Larson et al., 1994; Smith et al., 1997) (Fig. 2).

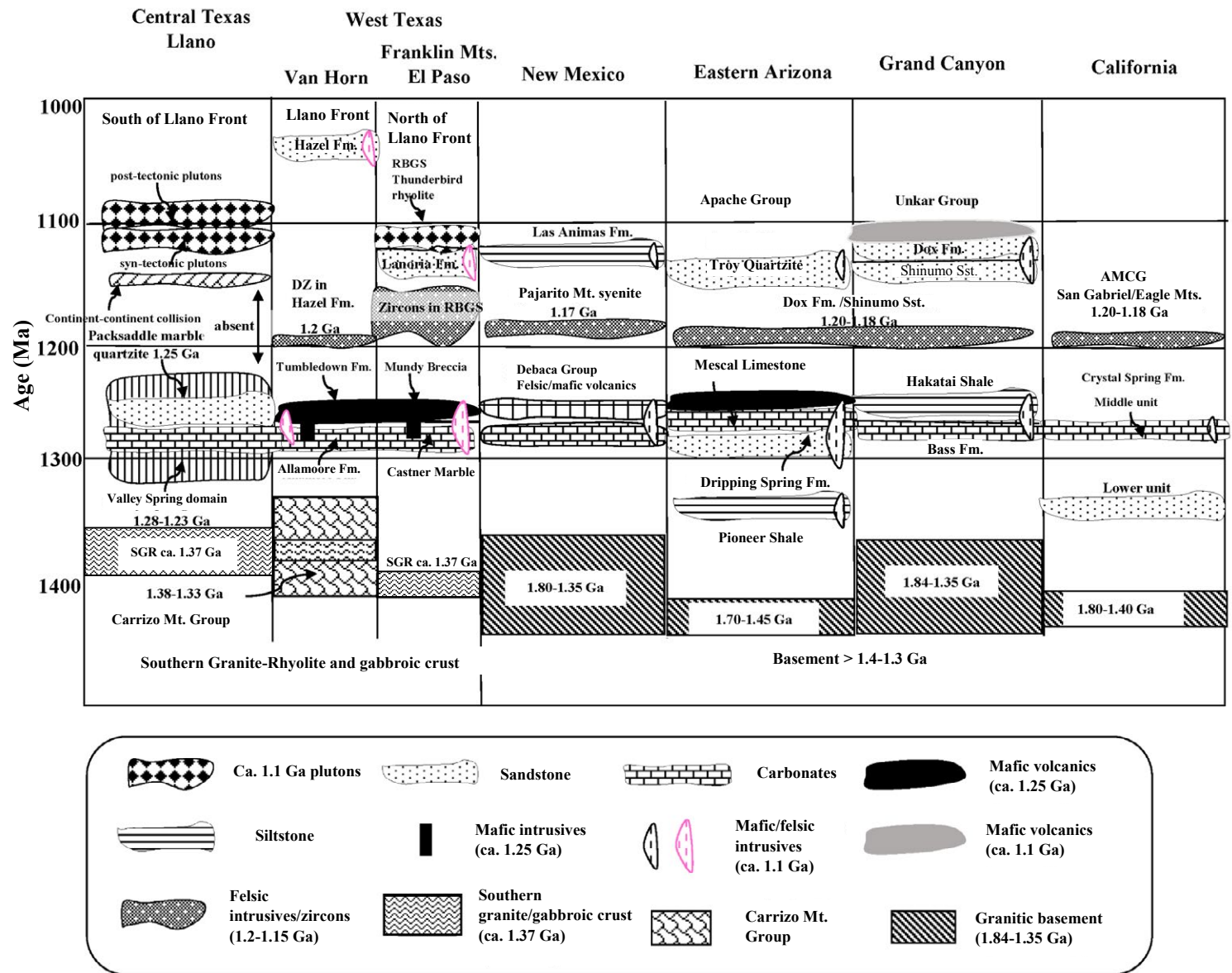


Figure 2. Regional stratigraphic correlation of Mesoproterozoic sedimentary deposits and associated magmatic rocks in southwestern Laurentia modified after Mulder et al. (2017) and references therein. AMCG— anorthosite-mangerite-charnockite-granite suite; DZ— detrital zircon; Fm.— Formation; RBGS— Red Bluff Granite Suite; SGR— Southern Granite-Rhyolite province; Sst.— Sandstone.

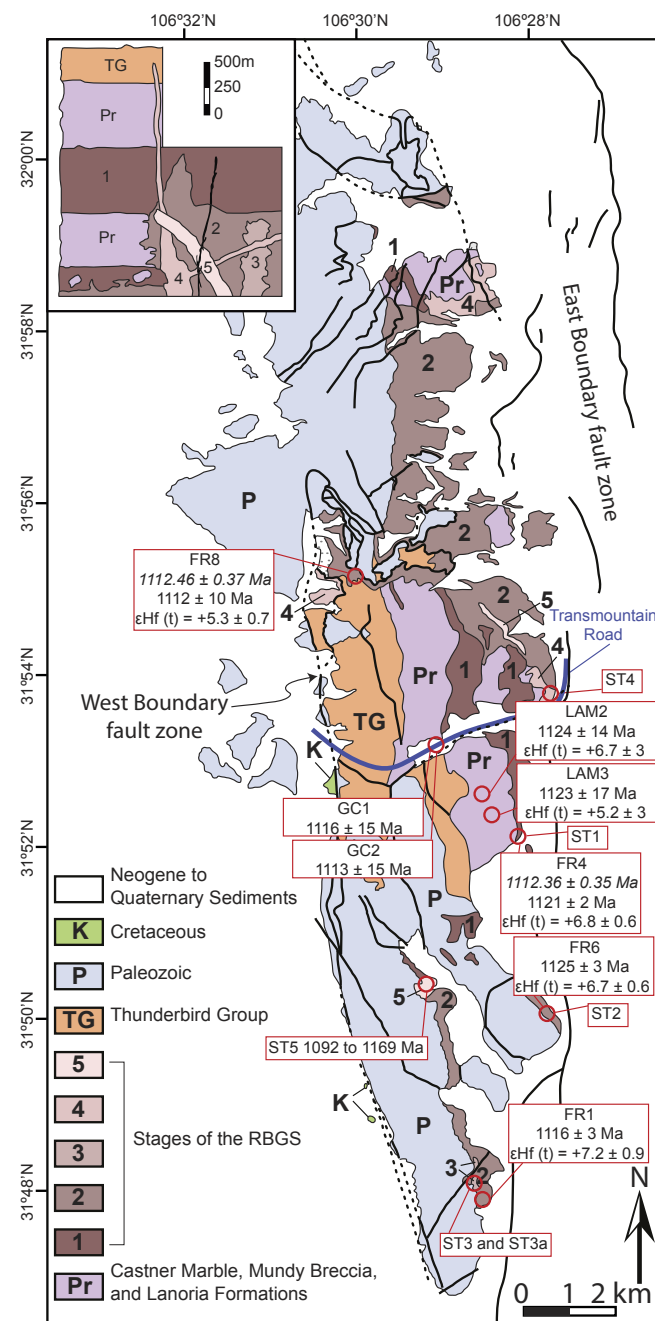
Li et al. (2007) reported similar basaltic sills and dikes, penetrated by the Mesalero well, Guadalupe County, New Mexico, and dated at 1105 Ma (Amarante et al., 2005). Bright et al. (2014) and Mulder et al. (2017) demonstrated that younger basaltic rocks are widespread throughout the southwestern United States, where they cut numerous rocks of the Mazatzal and Yavapai provinces as well as 1.1 Ga plutonic rocks (see Fig. 2).

LOCAL GEOLOGICAL SETTING OF THE FRANKLIN MOUNTAINS

The Franklin Mountains are the southernmost in a series of north-south-trending mountains extending from central Colorado to the westernmost tip of Texas (Figs. 1 and 3). The Castner Marble is the oldest exposed unit and is composed of intertidal-subtidal stromatolitic limestone, rhythmite, conglomerate, and tuffaceous siltstone (Pittenger et al., 1994). Zircons separated from a metatuff interbedded within the Castner Marble yielded a U-Pb age of 1260 ± 20 Ma (Pittenger et al., 1994). Bickford et al. (2000) also analyzed zircon grains from metatuff beds within the Castner Marble, and they reported upper intercept ages of 1251 ± 47 and 1272 ± 5 Ma. Subaqueous basaltic rocks of the Mundy Breccia overlie the Castner Marble (Pittenger et al., 1994) (Fig. 3). The Mundy Breccia has been interpreted as a volcanic agglomerate (Harbour 1960, 1972), weathered basalt lava flow or sill (Harbour, 1960, 1972), basalt flow breccia (Pittenger et al., 1994), or subaqueous flow breccia (Mulder et al., 2017). The Lanoria Formation unconformably overlies the Mundy Breccia and is composed of quartz arenite, subarkose, and mudstone (Seeley, 1999). These older rocks are exposed only as roof pendants within the younger RBGS (Seeley, 1999).

Next in the sequence is the RBGS, which is subdivided into five stages of magma injection on the basis of cross-cutting relationships and differences in mineralogy and texture (e.g., Shannon et al., 1997) (Fig. 3). In the following section, we briefly describe these magmatic stages; for a detailed mineralogical description for all five stages, see Shannon et al. (1997) and Barnes et al. (1999). Stage 1 rocks were initially termed microgranite by McAnulty (1967) because quartz is visible only in thin sections. They are gray to dark gray and holocrystalline and range compositionally from porphyritic granite to quartz syenite with large microcline glomerophenocrysts. In outcrop, stage 1 is composed of two separate north-south-trending sills in the Lanoria Formation and Castner Marble (Fig. 3B). The upper sill is granophyric biotite-hornblende granite, and

Figure 3. (A) Geological map of Franklin Mountains, west Texas, showing locations of studied granite and mafic dikes. **(B)** Schematic representation of intrusive sequence of Red Bluff Granite Suite (RBGS) after Anthony et al. (1991). Stage 1, alkali-feldspar quartz syenite to porphyritic alkali-feldspar granite; stage 2, alkali-feldspar granite; stage 3, alkali-feldspar quartz syenite; stage 4, leucogranite; stage 5, arfvedsonite granite (pegmatite); thicker black lines are ferrobasaltic dikes. Mineralogical composition of RBGS granite stages is after Shannon et al. (1997) and this study. Weighted mean ages shown in italics are calculated from the high-precision zircon U-Pb dates determined by using CA-ID-TIMS (chemical abrasion-isotope dilution-thermal ionization mass spectrometry).



the lower quartz syenite sill has large gray to dark gray alkali-feldspar crystals in the matrix. Bickford et al. (2000) assigned an upper intercept age of 1120 ± 35 to the stage 1 syenite. This age is comparable to those reported for rhyolite boulders and cobbles in the Hazel Formation in the Van Horn, Texas, area (Bickford et al., 2000). Stage 2 is represented by the most voluminous alkali-feldspar granites (Fig. 3), which show variable mineral assemblages. These intrusive rocks are exposed along the entire 20 km north-south stretch of the Franklin Mountains (Fig. 3). The granite is holocrystalline, is medium to coarse grained, and contains abundant perthitic alkali feldspar. Quartz, albitic plagioclase, biotite, fluorite, amphibole, and clinopyroxene are interstitial minerals. Ilmenite, magnetite, and apatite inclusions within amphibole are also present (Shannon et al., 1997). Stage 3 is represented by a dark, coarse-grained, holocrystalline biotite-hornblende quartz syenite. In outcrop, it is limited to small, isolated patches in the southern part of the Franklin Mountains (Fig. 3). The syenite is composed primarily of subhedral alkali feldspar, quartz, biotite, plagioclase, and amphibole. Interstitial and accessory minerals are similar to those of the rocks of stage 2. Stage 4 is represented by a fine-grained leucocratic (light gray to pink), porphyritic, and holocrystalline biotite-alkali feldspar granite with a fine-grained matrix. The phenocrysts are exclusively light gray to milky white subhedral crystals of alkali feldspar within a groundmass composed of quartz and alkali feldspar. Biotite and hornblende do not exceed 2%. Finally, stage 5 rocks consist of leucocratic, holocrystalline, medium- to very coarse-grained pegmatite dikes. The pegmatite contains black, subhedral, prismatic crystals of mostly riebeckite and minor amounts of black platy biotite and zircon in a leucocratic matrix consisting of alkali feldspar, quartz, and plagioclase. The alignment of the prismatic riebeckite crystals gives a banded appearance.

The Thunderbird Group, the youngest in the Proterozoic stratigraphic sequence, overlies the Lanoria Formation and consists of tuffs, volcanic conglomerates, rhyolitic ignimbrites, and porphyritic trachytes (Thomann and Hoffer, 1991). The Thunderbird rhyolite yielded a zircon U-Pb age of 1111 ± 20 Ma

(Roths, 1993). On the basis of comparable ages, it has been proposed that the Thunderbird rhyolite is likely the erupted equivalent of the intrusive RBGS (Norman et al., 1987; Roths, 1993; Shannon et al., 1997).

Proterozoic mafic dikes and sills of thickness ranging from a few centimeters to 9 m are present throughout the Franklin Mountains and are considered the youngest magmatic rocks in the Franklin Mountains (e.g., Harbour, 1960; Shannon et al., 1997). These dikes were identified as diabase as well as basalt; however, for the sake of simplicity, we refer to them here as basaltic dikes.

Figure 3B presents the cross-cutting relationships of the different magmatic stages of the RBGS. Both the Castner Marble and Mundy Breccia were intruded by the stage 1 syenite of the RBGS (details of these magmatic stages are given below). It should be noted that the stage 4 granite intrudes the entire Proterozoic stratigraphic sequence, including the Thunderbird Rhyolite Group (Fig. 3B). Therefore, the Thunderbird rhyolite is older than stage 4, perhaps having erupted during the emplacement of stage 3 and/or stage 2 granitoids. However, due to the larger uncertainty in the ages described above, the temporal relation between the RBGS and Thunderbird Rhyolite Group remains uncertain. All granite stages as well as sedimentary Proterozoic sequences are cut by the basaltic dikes, including the Castner Marble, Mundy Breccia, and Lanoria Formation (Fig. 3) (Harbour, 1960, 1972; Anthony et al., 1991; Thomann and Hoffer, 1991; Pittenger et al., 1994; Shannon et al., 1997) (Figs. 3B and 4). Based on composition, Shannon et al. (1997) interpreted these dikes as a late-stage ferrobasalt composed of phenocrysts of olivine and titanite in a groundmass of plagioclase laths, along with minor ilmenite and apatite.

RED BLUFF GRANITE SUITE AND SAMPLE DESCRIPTION

Sample FR4 was collected from the stage 1 holocrystalline quartz syenite from the east-central part of the Franklin Mountains (Fig. 3). The thin section

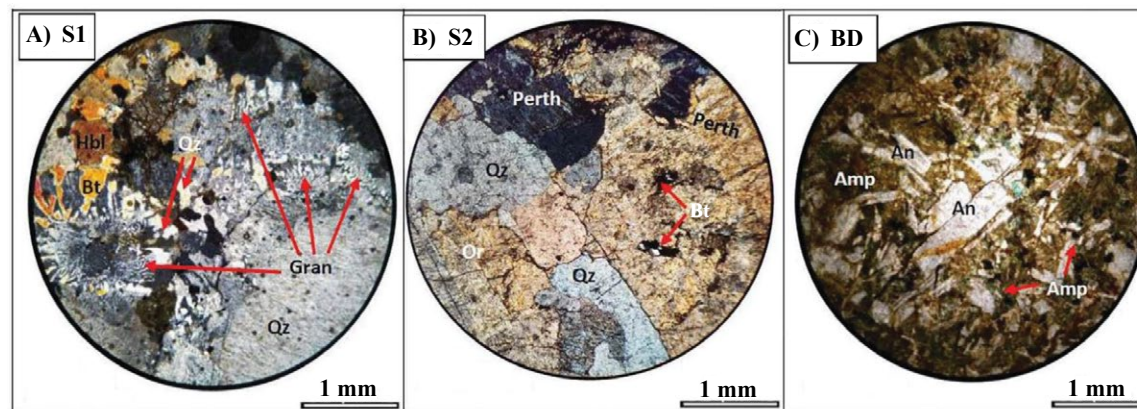


Figure 4. Photomicrographs of studied granites and basaltic dike. (A) Stage 1 (S1) granite shows granophyric texture. (B) Perthitic, intergrowths of feldspar can be observed in Stage 2 (S2) granite. (C) Basaltic dikes (BD) are composed predominantly of plagioclase and amphibole. Abbreviations: Amp—amphibole; An—anorthite; Bt—biotite; Gran—granophyric texture; Hbl—hornblende; Or—orthoclase; Perth—perthitic texture; Qtz—quartz.

shows characteristic blue prismatic arfvedsonite, cross-hatched microcline, perthite, and well-developed albite twinning. Large, anhedral, highly fractured, very fine-grained quartz and K-feldspar are the predominant minerals and granophyric texture (Fig. 4A). Phenocrysts are typically interlocking glomeroporphyritic aggregates of perthitic alkali feldspar within a groundmass of predominantly quartz and microcline (Fig. 4A). Three samples (FR1, FR6, and FR8) are from alkali-feldspar quartz syenite of stage 2. Samples FR1 and FR6 were collected from the south, while FR8 represents the north-central part of the Franklin Mountains (Fig. 3). Microscopically, samples show glomeroporphyritic texture (Fig. 4B). Feldspar is euhedral to subhedral and shows Carlsbad twinning. Such mineralization might represent the role of post-magmatic fluids because of the scarcity of pegmatite and estimates of water content (as much as 0.3 wt%) that indicate water-undersaturated magmatic conditions (Shannon et al., 1997). Samples ST1, ST2, ST3, ST3a, ST4, and ST5 are from stages 1 through 5 (Fig. 3) (sample numerals correspond to the stage numbers). Two samples, GC1 and GC2, are from a brecciated clastic dike intruding the Castner Marble along Transmountain Road (Loop 375) (Fig. 3). These angular, pink to greyish pink, medium- to coarse-grained brecciated clasts vary in size from 1 to 5 cm and are granitic in composition. Compositionally, granite clasts are composed primarily of alkali feldspar, quartz, minor biotite, and amphibole.

In addition to granitic rocks, two samples from basaltic dikes, LAM2 and LAM3, were collected from the central part of the Franklin Mountains (Fig. 3). These dikes have a maximum surface exposure with a length of 21 m and a width of 1.2 m. The dikes weather to a reddish-brown (rust) color, and a few sections of the larger outcrops display spheroidal weathering. The ferrobasaltic dikes are composed of plagioclase, clinopyroxene, and amphibole, have glomeroporphyritic texture, and contain mafic and plagioclase phenocrysts. The plagioclase phenocrysts are as large as 2 cm and exhibit Carlsbad twinning; phlogopite phenocrysts as large as 1.5 cm were also observed. Thin sections show opaque anhedral grains (Fe-Ti oxides) (Fig. 4C). Subophitic plagioclase laths are present with interstitial pyroxene, accessory ilmenite, and magnetite.

Zircon U-Pb ages were determined for samples FR4, FR1, FR6, FR 8, ST5, GC1, GC2, LAM2, and LAM3 using LA-MC-ICP-MS U-Pb geochronology. Hf isotopic compositions of selected zircons were determined for samples FR4, FR1, FR6, FR8, LAM2, and LAM3 using LA-MC-ICP-MS. High-precision U-Pb zircon CA-ID-TIMS ages were determined for samples FR4 and FR8. Samples ST1, ST2, ST3, ST3a, and ST4 were analyzed only for whole-rock geochemistry.

ANALYTICAL METHODS

Whole-rock geochemical analyses were performed by Activation Laboratories (Actlabs) in Ancaster, Ontario, Canada, using methods described on their website (<https://actlabs.com/geochemistry/lithochem/geochemistry-and-whole-rock-analysis/>). Lithium metaborate–lithium tetraborate fusion ICP-MS was employed to determine major elements, trace elements, and rare earth

elements (REEs). The zircon U-Pb and zircon Hf isotopic measurements were performed using laser ablation–multicollector–inductively coupled plasma–mass spectrometry (LA-MC-ICP-MS) at the Arizona LaserChron Center, University of Arizona, Tucson. The analytical methods for U-Pb and Hf isotopic data collected from zircons are fully described by Gehrels et al. (2008), Gehrels and Pecha (2014), and Cecil et al. (2011). Details of the methods are given in File S1 in the Supplemental Material¹. Individual U-Pb analyses listed in Table S1 are reported at 1 σ . Before analysis, zircons were imaged by cathodoluminescence (CL) at the LaserChron scanning electron microscope (SEM) lab facility. The final weighted mean ages, reported at 2 σ , include the instrumental as well as the systematic error. Systematic error is added to the instrumental error quadratically. Because all the samples in this study yielded older ages (≥ 1000 Ma), $^{206}\text{Pb}/^{207}\text{Pb}$ ages are considered the best age. Systematic error at 2 σ in $^{206}\text{Pb}/^{207}\text{Pb}$ ages is 0.8% and 0.6% for granites and basaltic dikes, respectively. The individual Hf isotopic compositions listed in Table S2 are reported at 1 σ . The weighted mean $\epsilon\text{Hf}(t)$ isotopic compositions are reported at a 95% confidence level with data-point error symbols at 1 σ .

High-precision U-Pb dates on single zircon grains were obtained by the chemical abrasion–isotope dilution–thermal ionization mass spectrometry (CA-ID-TIMS) method at the Boise State University Isotope Geology Laboratory, Boise, Idaho, USA, modified after Mattinson (2005). Individual U-Pb analyses are listed in Table S3 (see footnote 1). A detailed description of CA-ID-TIMS U-Pb geochronology methods is provided in File S1. Weighted mean ages were calculated from multiple single zircon dates using IsoPlot 3.0 (Ludwig, 2003). Crystallization ages are interpreted from $^{206}\text{Pb}/^{238}\text{U}$ dates because they are more precise than $^{207}\text{Pb}/^{206}\text{Pb}$ dates and there is no evidence for Pb loss; discordance is 0.04%–0.24%. Error is given at the 95% confidence interval.

RESULTS

Whole-Rock Geochemistry

Samples were collected from unaltered fresh rocks, as reflected in their low loss on ignition (LOI) of <1.5 except for sample LAM2 which has a higher LOI of 1.9. Eight new analyses (Table 1) and 20 published analyses of Shannon et al. (1997) are plotted in Figures 5 and 6. The RBGS granites are marginally metaluminous. On the $Q' = 100 \times Qz / (Qz + Ab + Or + An)$ versus $ANOR = 100 \times An / (An + Or)$ (where Qz is quartz, Ab is albite, Or is orthoclase, and An is anorthite) classification diagram of Streckeisen and LeMaitre (1979), modified by Whalen and Frost (2013) for magma evolution trends, all the granite samples plot along the alkalic trendline (Fig. 5A). Samples from stages 2, 4, and 5 fall

¹Supplemental Material. Contains description of analytical methods, plotweighted mean $\epsilon\text{Hf}(t)$ of studied samples, cathodoluminescence (CL) images and backscattered electron (BSE) images of 18 selected zircons. Excel files contain geochronology and Hf isotopic data tables. Please visit <https://doi.org/10.1130/GEOS.S.21717899> to access the supplemental material, and contact editing@geosociety.org with any questions.

TABLE 1. WHOLE-ROCK GEOCHEMICAL DATA OF STAGES OF RED BLUFF GRANITE SUITE AND ASSOCIATED MAFIC DIKES

Sample name	Red Bluff Granite Suite						Mafic dike	
	ST1	ST2	ST3	ST3a	ST4	ST5	LAM2	LAM3
<u>Major oxides (wt%)</u>								
SiO ₂	67.1	67.2	71.5	71.4	75.2	69.8	48.6	48.7
Al ₂ O ₃	15.3	14.8	12.5	12.7	12.4	11.8	13.8	13.7
Fe ₂ O ₃ (Total)	3.3	4.8	4.2	3.7	0.9	5.7	15.4	15.7
MnO	0.1	0.1	0.1	0.1	0.0	0.2	0.2	0.2
MgO	0.2	0.1	0.1	0.1	0.0	0.0	3.4	3.5
CaO	1.3	0.7	0.8	1.1	0.8	0.1	9.2	9.0
Na ₂ O	5.0	4.2	3.9	4.0	3.8	2.6	1.8	1.8
K ₂ O	5.8	5.9	5.5	5.1	5.1	8.0	2.2	2.4
TiO ₂	0.3	0.3	0.3	0.3	0.1	0.0	3.5	3.4
P ₂ O ₅	0.1	0.0	0.0	0.0	<0.01	<0.01	0.6	0.5
LOI (loss on ignition)	0.7	1.3	0.9	1.2	0.8	0.4	1.9	1.3
Total	99.2	99.4	99.6	100.1	99.1	98.6	100.6	100.2
<u>Trace elements (ppm)</u>								
Sc	4	2	2	2	<1	3	37	38
Be	5	8	8	14	17	11	2	2
V	<5	<5	<5	<5	<5	<5	401	389
Cr	<20	<20	<20	<20	<20	<20	<20	<20
Co	<1	<1	<1	<1	<1	<1	25	27
Ni	<20	<20	<20	<20	<20	<20	<20	20
Cu	<10	<10	<10	<10	<10	<10	<10	<10
Zn	50	60	160	200	<30	610	200	220
Ga	35	46	34	34	34	52	25	26
Ge	3	2	2	2	2	5	2	2
As	<5	<5	26	<5	<5	<5	<5	<5
Rb	174	220	218	220	371	>1000	102	112
Sr	82	27	35	23	22	40	270	280
Y	139	215	166	197	102	313	58	59
Zr	326	1209	980	936	176	275	317	308
Nb	38	81	50	55	47	23	18	19
Mo	<2	3	3	3	<2	<2	<2	<2
Ag	1.2	4	3.5	3.3	0.6	0.9	1.1	1.1
In	0.2	0.3	<0.2	<0.2	<0.2	2.3	<0.2	<0.2
Sn	5	14	9	7	3	83	4	3
Sb	<0.5	<0.5	<0.5	<0.5	<0.5	<0.5	0.9	0.9
Cs	<0.5	1.3	4.7	1.1	0.9	3.2	9	10.5
Ba	674	328	330	266	125	188	860	899
La	165	166	132	130	47.9	47	30.3	31.9
Ce	361	365	296	297	130	174	72.7	75.5
Pr	55.8	44.2	36.7	35.9	15.6	24.5	10.3	10.3
Nd	227	166	141	136	53.1	87.5	47	46.2
Sm	49.3	35.7	30.8	29.9	12.3	34.8	11.9	11.8
Eu	2.31	2.72	2.17	1.94	0.48	1.13	3.6	3.6
Gd	40.6	32	28.4	27.6	9.5	40.9	12.1	11.9
Tb	6.2	5.9	4.9	5.3	2	10.2	2	2
Dy	34.8	38.3	30.9	33.4	14.3	68.9	12	11.7

(continued)

TABLE 1. WHOLE-ROCK GEOCHEMICAL DATA OF STAGES OF RED BLUFF GRANITE SUITE AND ASSOCIATED MAFIC DIKES (*continued*)

Sample name	Red Bluff Granite Suite						Mafic dike	
	ST1	ST2	ST3	ST3a	ST4	ST5	LAM2	LAM3
Ho	6.1	7.8	6.3	6.8	3.3	13.2	2.4	2.3
Er	16.3	23.4	18.3	20.4	11.3	34.6	6.9	6.7
Tm	2.2	3.62	2.66	3.21	2.09	4.53	0.99	0.94
Yb	14.2	24.2	17.1	21.0	14.8	25.3	6.4	6.1
Lu	2.08	3.59	2.52	3.13	2.35	3.44	0.99	0.96
Hf	9.6	29.8	23.1	23.0	8.5	13.8	7.8	7.9
Ta	4.5	7.2	4.0	3.7	5.8	1.2	1.3	1.3
W	<1	<1	1.0	2.0	1.0	<1	<1	<1
Ti	0.02	0.4	0.5	0.5	0.7	2.0	0.9	0.9
Pb	13	8	24	19	8	6	18	28
Bi	<0.4	<0.4	<0.4	<0.4	<0.4	<0.4	<0.4	<0.4
Th	25.2	31.3	26.2	40.6	47.7	11.3	4.1	4.2
U	3.7	6.5	4.9	5.3	9.4	2.3	1	1

exclusively in the alkali-feldspar granite field. Samples from stages 1 and 3 fall within the alkali-feldspar quartz syenite and syenogranite fields. It appears that the source magma progressively evolved from alkali-feldspar quartz syenite and/or alkali-feldspar syenite to alkali-feldspar granite composition. All granite samples show typical ferroan character with $\text{FeO}^{\text{total}}/(\text{FeO}^{\text{total}} + \text{MgO}) > 0.9\text{--}1.0$ (Fig. 5B). On the modified alkali-lime index (MALI; $\text{Na}_2\text{O} + \text{K}_2\text{O} - \text{CaO}$) versus SiO_2 diagram, samples show alkali to alkali-calcic trends consistent with the Q-ANOR tectonomagmatic diagram (Fig. 5C). Mafic dikes show a ferroan, calc-alkalic to alkali-calcic character (Figs. 5B and 5C). On the tectonic discrimination diagram of Whalen and Hildebrand (2019), all the samples fall in the A-type field (Fig. 5D) and can be further classified as A2-type granites (Fig. 5E).

Except for one sample from stage 4, all granite samples show elevated high field strength element (HFSE) compositions (i.e., Zr + Nb + Ce + Y ranging from 785 to 1870 ppm), a typical characteristic of A2-type granitoids (Table 1). The primitive mantle-normalized REE compositions (Fig. 6A) show slight enrichment in light REEs (LREEs), a strong negative Eu anomaly, and a flatter heavy REE (HREE) pattern. Also, Ba, Sr, P, and Ti show strong negative anomalies (Fig. 6B). A2-type enriched HFSE compositions of basaltic dikes suggest their formation in a post-orogenic setting instead of an anorogenic, within-plate environment. Depletions in Ba, Sr, P, Ti, and Eu in the granites indicate fractionation of feldspar, apatite, ilmenite, and magnetite.

Zircon Morphology

Zircons from the RBGS are 100–500 microns in length and are typically euhedral but rarely subhedral. Backscattered electron and CL images of selected zircons are shown in File S1 (see footnote 1). Zircon grains from stage 2 granitoids of the RBGS show convolute zoning textures, most notably

in the interior of the grains. Zircons extracted from mafic dikes are euhedral to subhedral with strong oscillatory zoning and have very similar morphology to the zircons from granitoids of the RBGS. Also, zircons from the RBGS and basaltic dikes yielded essentially identical U-Pb ages, overlapping $\text{eHf}(t)$, and depleted mantle model ages. This coupled with zircon inheritance of 1164–1260 Ma in basaltic dikes suggests that all the zircons in the basaltic dikes are xenocrysts and were derived from the host granites. Therefore, zircons found in basaltic dikes will be treated as xenocrystic zircons from the host RBGS. Zircons from the brecciated granite dike showed similar morphology to that of other granites. Some zircons have broad bright cores with no zoning, while others show convolute and oscillatory zoning.

LA-MC-ICP-MS U-Pb Geochronology

Concordia plots with $^{206}\text{Pb}/^{207}\text{Pb}$ weighted mean ages are shown in Figure 7 and summarized in Table 2. Concordia ages were calculated from a coherent group of concordant dates (i.e., <2%–3% discordance). The U-Pb data for all the samples are provided in Table S1 (see footnote 1); backscattered electron and CL images of selected zircons are shown in Figure S1 of File S1.

Stage 1 quartz syenite sample FR4 yielded a concordia age of 1123 ± 3 Ma (mean square of weighted deviates [MSWD] = 0.96, $n = 12$). Samples FR6 and FR8 from stage 2 alkali-feldspar granite yielded concordia ages of 1122 ± 5 (MSWD = 0.088, $n = 6$) and 1105 ± 5 (MSWD = 2.1, $n = 10$), respectively. Sample FR1 from stage 2 yielded an upper intercept age of 1123 ± 7 Ma (MSWD = 0.95, $n = 6$). Sample ST5 from the stage 5 biotite–arfvedsonite–alkali feldspar granite yielded few zircons; three analyses yielded individual dates from 1169 to 1092 Ma. Two samples, GC1 and GC2, from the brecciated granite dikes yielded concordia ages of 1114 ± 8 (MSWD = 0.04, $n = 9$) and 1111 ± 9 Ma (MSWD = 0.12,

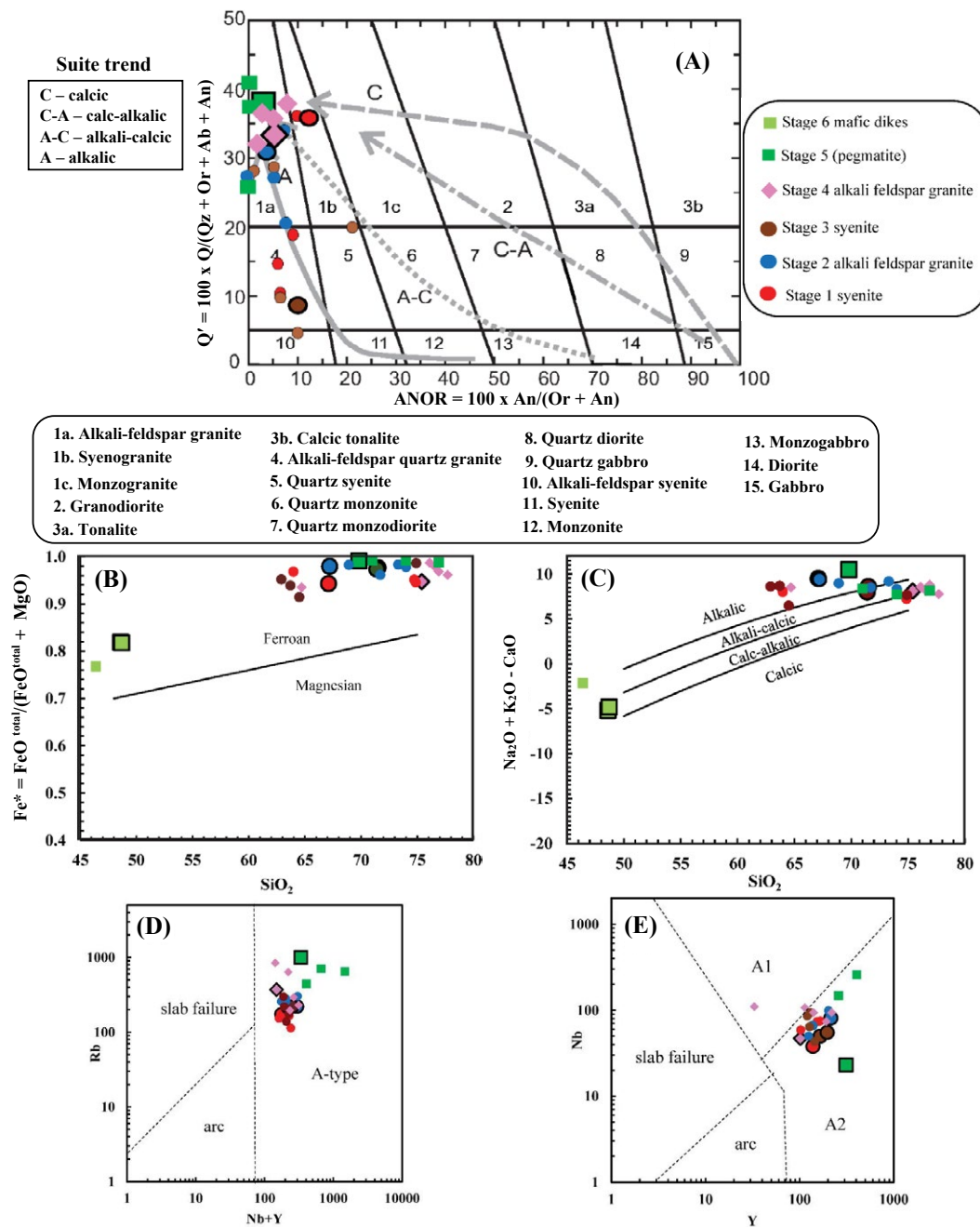


Figure 5. Plots of Red Bluff Granite Suite stages. (A) Q' versus ANOR classification diagram, as modified by Whalen and Frost (2013). (B and C) Fe* versus SiO₂ and modified alkali-lime index (MALI; Na₂O + K₂O - CaO) versus SiO₂ plots (Frost et al., 2001). Abbreviations: Ab—albite; An—anorthite; Or—orthoclase; Qz—quartz. (D and E) Tectonomagmatic plots after Whalen and Hildebrand (2019). Data from Shannon et al. (1997) are included. Larger symbols with dark borders are from this study.

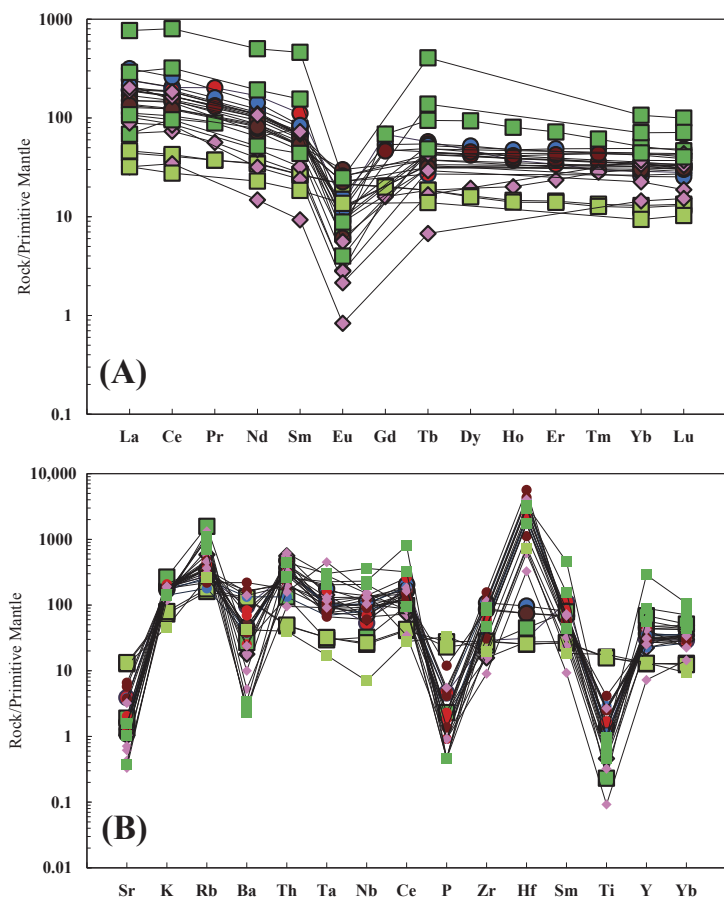


Figure 6. Chondrite-normalized rare earth element (A) and trace element (B) patterns of Red Bluff Granite Suite (symbols are same as shown in Fig. 5).

$n = 9$), respectively. Within the relatively large uncertainty of the LA-MC-ICP-MS methods, the dates from all the granitic rocks are irresolvable.

Zircons that yielded dates older than ca. 1130 Ma are interpreted as being inherited grains. Samples FR4, FR1, FR6, and FR8 yielded the oldest individual dates of 1148 ± 25 , 1130 ± 17 , 1138 ± 15 , and 1138 ± 48 Ma, respectively. Sample GC1 yielded older individual dates of 1195 ± 23 , 1300 ± 61 , 1306 ± 30 , and 1362 ± 62 Ma. Sample GC2 yielded dates of 1193 ± 18 , 1234 ± 16 , 1283 ± 33 , and 1312 ± 71 Ma. Zircons found in the two basaltic dike samples LAM2 and LAM3 are xenocrystic. Twelve out of 15 analyses from LAM2 yielded $^{206}\text{Pb}/^{207}\text{Pb}$ concordant (<5% discordance) dates varying from 1095 ± 22 to 1154 ± 23 Ma (Fig. 7G); one zircon yielded a concordant date of 1164 ± 29 Ma, and

two zircon grains yielded discordant (17% discordance) $^{206}\text{Pb}/^{207}\text{Pb}$ dates of 1075 ± 20 and 1260 ± 32 Ma. Seven out of eight analyses from LAM3 yielded $^{206}\text{Pb}/^{207}\text{Pb}$ concordant dates (<5% discordance) ranging from 1085 ± 20 to 1155 ± 23 Ma; one xenocrystic zircon yielded an older $^{206}\text{Pb}/^{207}\text{Pb}$ concordant (<2% discordance) date of 1216 ± 17 Ma (Fig. 7H). The majority of these dates are similar to those of the zircons found in granite samples.

CA-ID-TIMS U-Pb Geochronology

We selected samples FR4 and FR8 from stage 1 and stage 2 granitoids, respectively, for high-precision CA-ID-TIMS U-Pb dating. Selected zircons are shown in Figure S2 of File S1 (see footnote 1). Zircon $^{206}\text{Pb}/^{238}\text{U}$ weighted mean dates and concordia plots are shown in Figure 8 and summarized in Table 2. The U-Pb data are given in Table S3.

Seven dates from sample FR4 yield a weighted mean $^{206}\text{Pb}/^{238}\text{U}$ of 1112.36 ± 0.35 Ma (MSWD = 1.7, probability of fit = 0.11). Six dates from sample FR8 yielded a weighted mean $^{206}\text{Pb}/^{238}\text{U}$ of 1112.46 ± 0.37 Ma (MSWD = 0.6, probability of fit = 0.69). The uncertainty in the calculated weighted mean ages is at 2σ . These overlapping dates are interpreted as igneous crystallization ages, and thus there is no discernable gap in the emplacement of the two granite stages.

LA-MC-ICP-MS Hf Isotopic Data

Weighted-mean Hf isotopic compositions of studied samples shown in File S1 (see footnote 1) and summarized in Table 2 are at a 95% confidence level. The initial Hf isotope compositions [$\epsilon\text{Hf}(t)$] of all the granite samples range from +3.3 to +9.2. Present-day Hf isotopic composition [$\epsilon\text{Hf}(0)$] of the RBGS varies from -13 to -18. The weighted mean $\epsilon\text{Hf}(t)$ compositions of zircons from four granite samples FR1, FR6, FR8, and FR4 are less variable at $+7.16 \pm 0.95$ (MSWD = 1.0, $n = 6$), $+6.72 \pm 0.62$ (MSWD = 0.58, $n = 13$), $+5.26 \pm 0.69$ (MSWD = 1.5, $n = 15$), and $+6.82 \pm 0.63$ (MSWD = 1.3, $n = 14$), respectively. The initial Hf isotope composition $\epsilon\text{Hf}(t)$ of xenocrystic zircons from samples LAM2 and LAM3 range from +2.1 to +12.9 with weighted mean $\epsilon\text{Hf}(t)$ of $+6.7 \pm 2.6$ (MSWD = 9.4, $n = 7$) and $+5.2 \pm 3.3$ (MSWD = 4.9, $n = 4$), respectively.

Single-stage depleted mantle model ages (T_{DM}) were calculated based on a model similar to that of Nowell et al. (1998), as discussed by Mueller et al. (2008) using the $^{176}\text{Lu}/^{177}\text{Hf}$ ratios of the zircons. Two-stage crustal model ages (Andersen et al., 2002) were calculated with a modified version of a program used in the Department of Geological Sciences, University of Florida (Gainesville, Florida, USA) laboratories. Two-stage crustal model ages Tcr1 and Tcr2 (i.e., crustal residence time) assumed continental crustal $^{176}\text{Lu}/^{177}\text{Hf} = 0.0083$ for upper continental crust or 0.015 for middle to lower crust, respectively (Rudnick and Gao, 2003).

Xenocrystic zircons from basaltic dike samples yielded average single-stage T_{DM} ages of ca. 1.36 Ga, whereas average two-stage crustal model ages

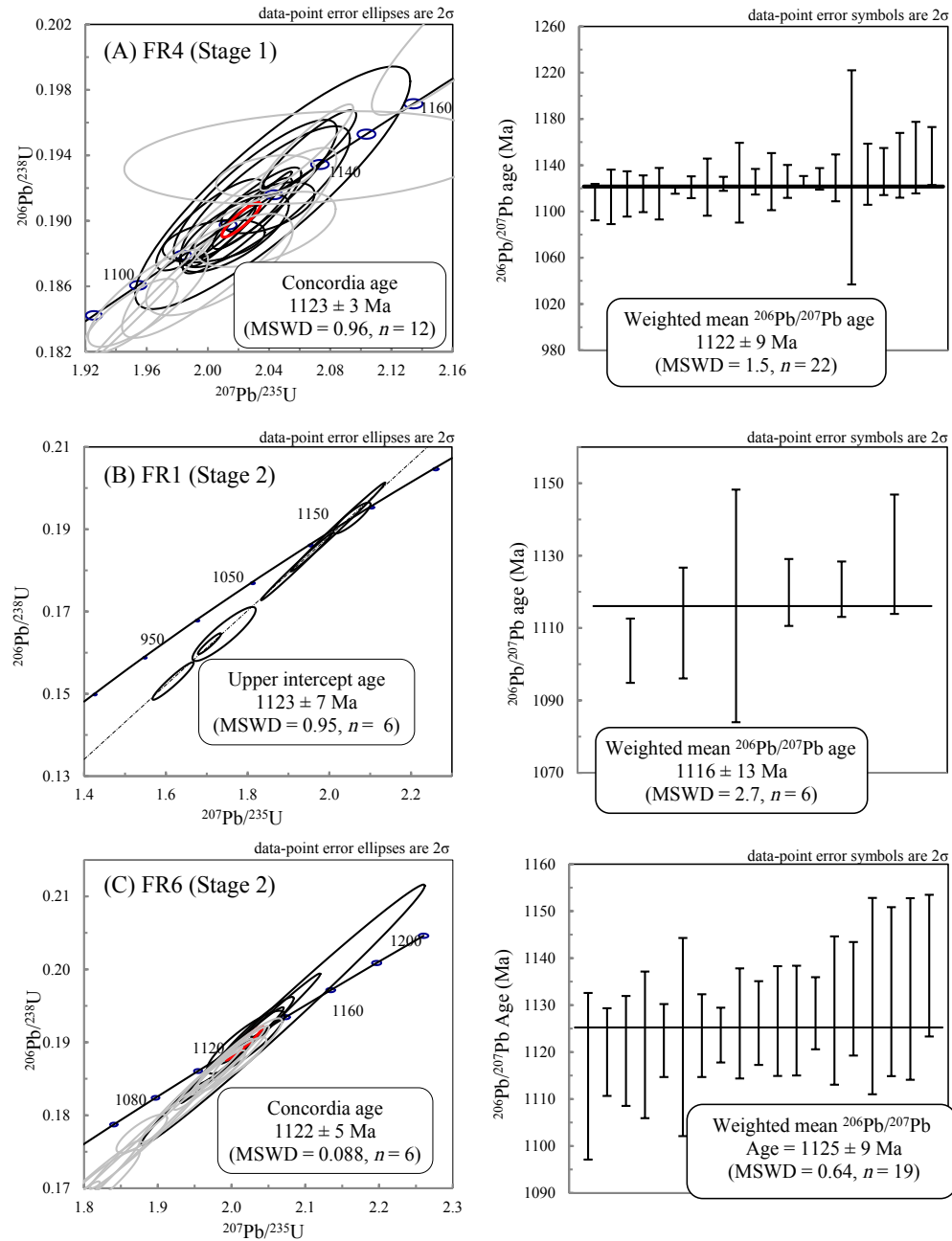


Figure 7. Concordia and $^{206}\text{Pb}/^{207}\text{Pb}$ age plots. All ages shown in the concordia plots are concordia ages except an upper intercept age calculated for sample FR1. MSWD—mean square of weighted deviates. Grey ellipses either are discordant ($\geq 3\%$ discordance) dates or do not constitute a single coherent age group. (Continued on the following 2 pages.)

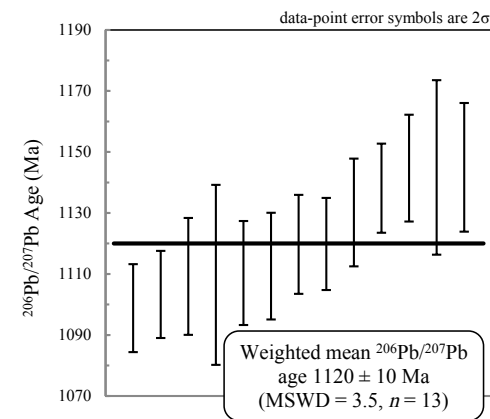
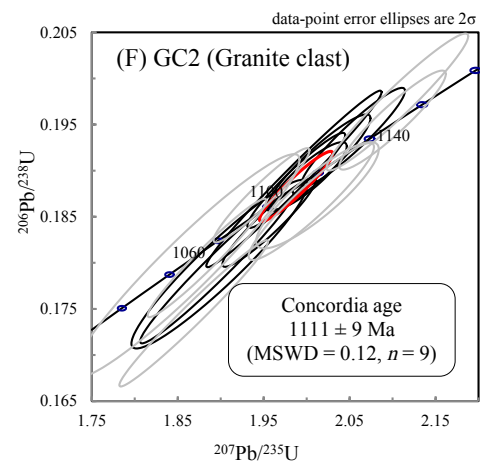
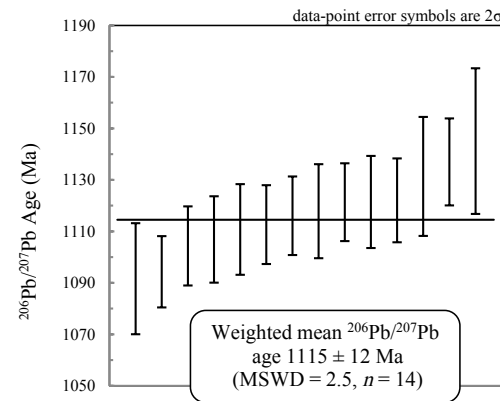
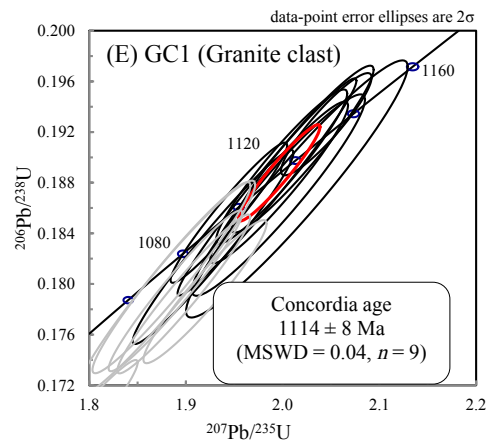
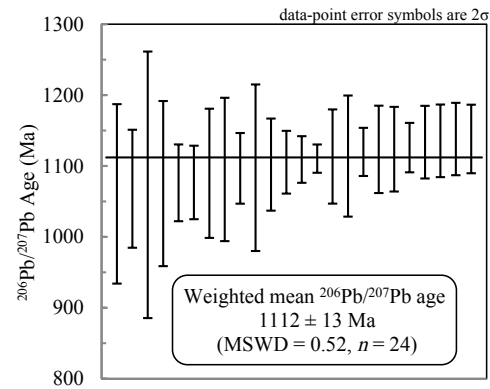
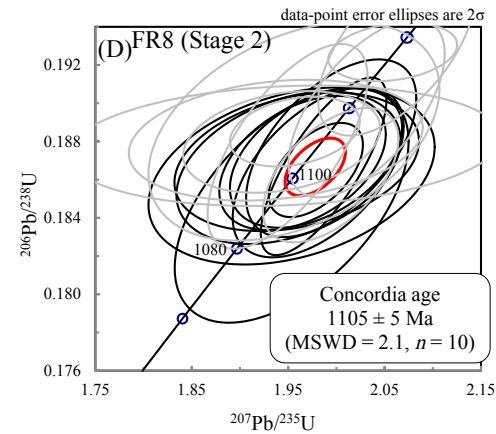


Figure 7. (Continued on the following page.)

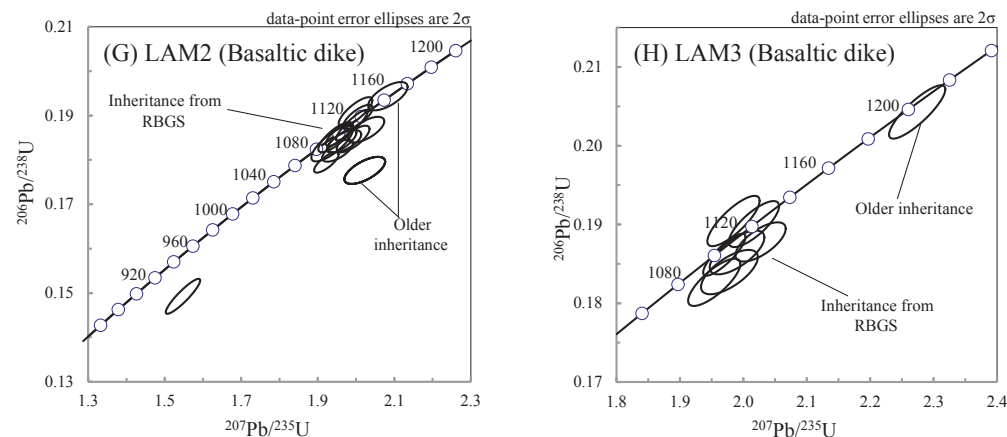


Figure 7 (Continued). RBGS—Red Bluff Granite Suite.

are ca. 1.35 and 1.41 Ga, assuming the whole-rock Lu/Hf ratios of the source magmas of 0.0083 and 0.015, respectively. Zircons from granite samples FR1, FR4, FR6, and FR8 yielded average single-stage T_{DM} ages of ca. 1.33, 1.35, 1.37, and 1.38 Ga, respectively, whereas average two-stage crustal model ages for these samples are ca. 1.37, 1.40, 1.39, and 1.43 Ga, respectively, for an assumed Lu/Hf ratio of 0.0083; average two-stage crustal model ages for a higher Lu/Hf ratio of 0.015 are ca. 1.43, 1.48, 1.47, and 1.52 Ga, respectively. Isotopic data and calculated model ages are given in Table S2 (see footnote 1).

Hafnium (Hf) isotopic compositions of the RBGS largely overlap with those of the temporally related Grenville magmatic rocks of the Llano Uplift and

granites within the Little Hatchet Mountains of New Mexico (1077 ± 4 Ma; Amato and Mack, 2012) and detrital zircons from the Grand Canyon (Howard, 2013; Hantsche, 2015; Mulder et al., 2017) (Fig. 9A).

Single-stage zircon Hf T_{DM} ages as well as two-stage crustal model ages from the RBGS vary from ca. 1.5 to 1.3 Ga (Fig. 9B). We also calculated Hf T_{DM} ages using the Hf isotopic data reported by Howard (2013) for 1.1 Ga rocks across the Grenville front from California to the Appalachians, including those exposed in west (RBGS) and central (Llano) Texas (Figs. 1 and 10A) (see Table S2, footnote 1). The Hf T_{DM} model ages of the RBGS and Llano rocks are indistinguishable and dominantly range from 1.5 to 1.3 Ga. The average Hf

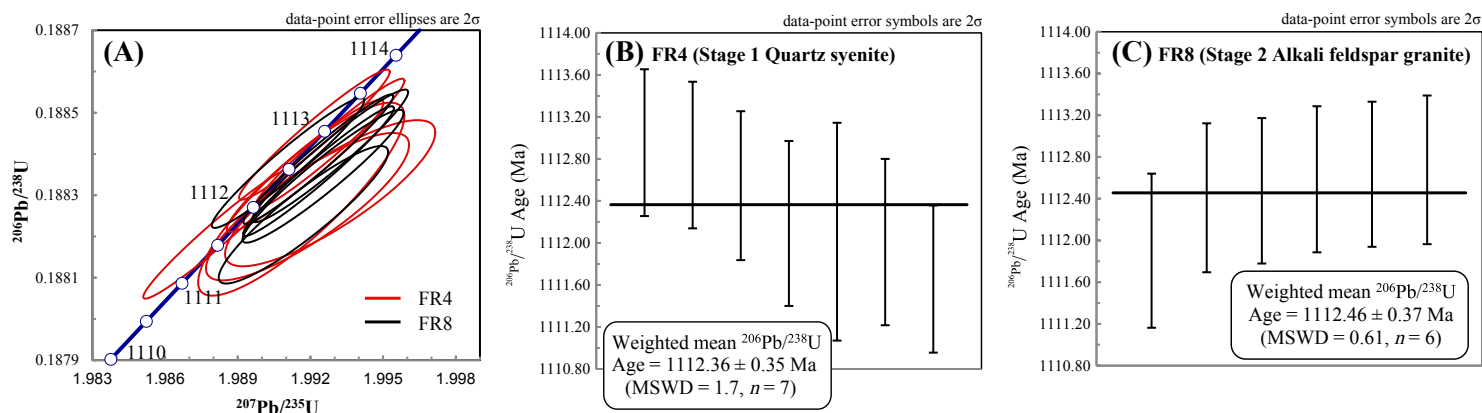


Figure 8. (A) Concordia plot of chemical abrasion–isotope dilution–thermal ionization mass spectrometry (CA-ID-TIMS) U–Pb dates from zircons. Error ellipses are at 2σ . (B and C) Weighted mean ages.

TABLE 2. SUMMARY OF ISOTOPIC AND GEOCHEMICAL DATA

Sample	Rock unit	Location	Concordia age* (Ma) (MSWD, n)	CA-ID-TIMS ²⁰⁶ Pb/ ²³⁸ U ages† (Age ± X/Y/Z) (Ma) (MSWD, n/N)	Xenocrystic inheritance (Ma)	Fe number	Alkalinity SiO ₂ versus K ₂ O	SiO ₂ (wt%)	Zircon initial εHf(t) (MSWD, n)
FR4	RBGS stage 1 (syenite)	31°52'1.2"N 106°27'50.4"W	1123 ± 3 Ma (0.96, 12)	1112.36 ± 0.35/0.46/1.20 (1.7, 6/7)	1147 and 1225	0.9	Shoshonite	67.1	+6.82 ± 0.63 (1.3, 14)
FR1 [§]	RBGS stage 2 (granite)	31°47'52.8"N 106°28'19.2"W	1123 ± 7 Ma (0.95, 6)	N.D.	N.D.	1.0	Shoshonite	67.2	+7.16 ± 0.95 (1.0, 6)
FR6	RBGS stage 2 (granite)	31°49'48.0"N 106°27'25.2"W	1122 ± 5 Ma (0.088, 6)	N.D.	N.D.	N.D.	N.D.	N.D.	+6.72 ± 0.62 (0.58, 13)
FR8	RBGS stage 2 (granite)	31°55'12"N 106°29'49.2"W	1105 ± 5 Ma (2.1, 10)	1112.46 ± 0.37/0.48/1.20 Ma (0.61, 6/6)	1178	N.D.	N.D.	N.D.	+5.26 ± 0.69 (1.5, 15)
ST5	RBGS stage 5 (granite)	31°50'22.8"N 106°29'9.6"W	1092 to 1169	N.D.	1168	1.0	Shoshonite	69.8	N.D.
GC1	Granite clast	31°53'38.9"N 106°28'14.2"W	1114 ± 8 Ma (0.04, 9)	N.D.	1195–1362	N.D.	N.D.	N.D.	N.D.
GC2	Granite clast	31°53'38.9"N 106°28'14.2"W	1111 ± 9 Ma (0.12, 9)	N.D.	1193–1312	N.D.	N.D.	N.D.	N.D.
LAM2	Basaltic dike	31°52'17.1"N 106°28'10.0"W	Not calculated	N.D.	1075–1260	0.8	Shoshonite	48.6	+6.7 ± 2.6 (9.4, 7)
LAM3	Basaltic dike	31°52'13.2"N 106°28'10.3"W	Not calculated	N.D.	1085–1216	0.8	Shoshonite	48.7	+5.2 ± 3.3 (4.9, 4)

Note: MSWD—mean square of weighted deviates; n—number of individual zircon dates included in the weighted mean age calculation; N—number of individual zircons analyzed for the sample; RBGS—Red Bluff Granite Suite; N.D.—no data. Errors on the ²⁰⁶Pb/²³⁸U weighted mean dates are given as ± X/Y/Z, where X is the internal error based on analytical uncertainties only, including counting statistics, subtraction of tracer solution, and blank and initial common Pb subtraction, Y includes the tracer calibration uncertainty propagated in quadrature, and Z includes the ²³⁸U decay constant uncertainty propagated in quadrature.

*Laser ablation–multicollector–inductively coupled plasma–mass spectrometry (LA-MC-ICP-MS) U-Pb geochronology.

†Chemical abrasion–isotope dilution–thermal ionization mass spectrometry (CA-ID-TIMS) U-Pb geochronology. Uncertainties in the CA-ID-TIMS weighted mean ages: X is 2σ analytical uncertainty; Y is 2σ uncertainty also incorporating tracer calibration for comparison to U-Pb dates not developed using EARTHTIME-calibrated tracer solutions (Condon et al., 2015); Z is 2σ uncertainty including X and Y, as well as ²³⁸U decay constant uncertainty (0.108%; Jaffey et al., 1971). The Z uncertainty needs to be utilized when comparing to dates using other decay systems (e.g., ⁴⁰Ar/³⁹Ar, ¹⁸⁷Re–¹⁸⁷Os).

§Sample FR1: upper intercept age; all other LA-MC-ICP-MS ages are concordia ages. Fe-number—FeO/(FeO + MgO).

T_{DM} model age of RBGS and Llano magmatic rocks is 1.38 ± 0.09 Ga. Southern Nevada and California also yield largely similar Hf T_{DM} ages of 1.5–1.3 Ga. Older zircon Hf T_{DM} model ages were observed only from Grenvillian gneisses (ca. 1.1 Ga) in the Appalachians. These ages vary predominantly from 1.4 to 1.5 Ga, with several ages ranging from 1.6 to 1.7 Ga.

Hafnium and Nd model ages (T_{DM}) for the RBGS and Llano rocks are largely restricted at ca. 1.3 Ga (Figs. 10A and 10B). Llano metamorphic rocks (emplacement age of 1.25–1.23 Ga) as well as syntectonic (1116 ± 2 to 1119 +6/–3 Ma) and post-tectonic granitoids (1070 ± 2 to 1093 ± 6 Ma) (Mosher, 1998, and references therein) yielded similar Nd model ages to those of the RBGS

(Patchett and Ruiz, 1089) (Fig. 10B). Both Hf and Nd model ages (Figs. 10A and 10B) for the 1.1 Ga magmatic rocks across the Grenville belt are all younger than 1.5 Ga; exceptions are Appalachian gneisses. On the other hand, 1.1 Ga Pikes Peak batholith (Colorado) granitoids intruding the Yavapai-Mazatzal basement yielded model ages >1.5 Ga, suggesting the involvement of older Mazatzal crust.

Hafnium isotopic data from west and central Texas (Fig. 9) are consistent with previous low Sr (0.7034–0.7062) and higher Nd isotopic values (+2.5 to +5) (Zartman, 1964, 1965; DeLong and Long, 1976; Garrison et al., 1979; Nelson and DePaolo, 1985; Patchett and Ruiz, 1989; Smith et al., 1997). Contrasting

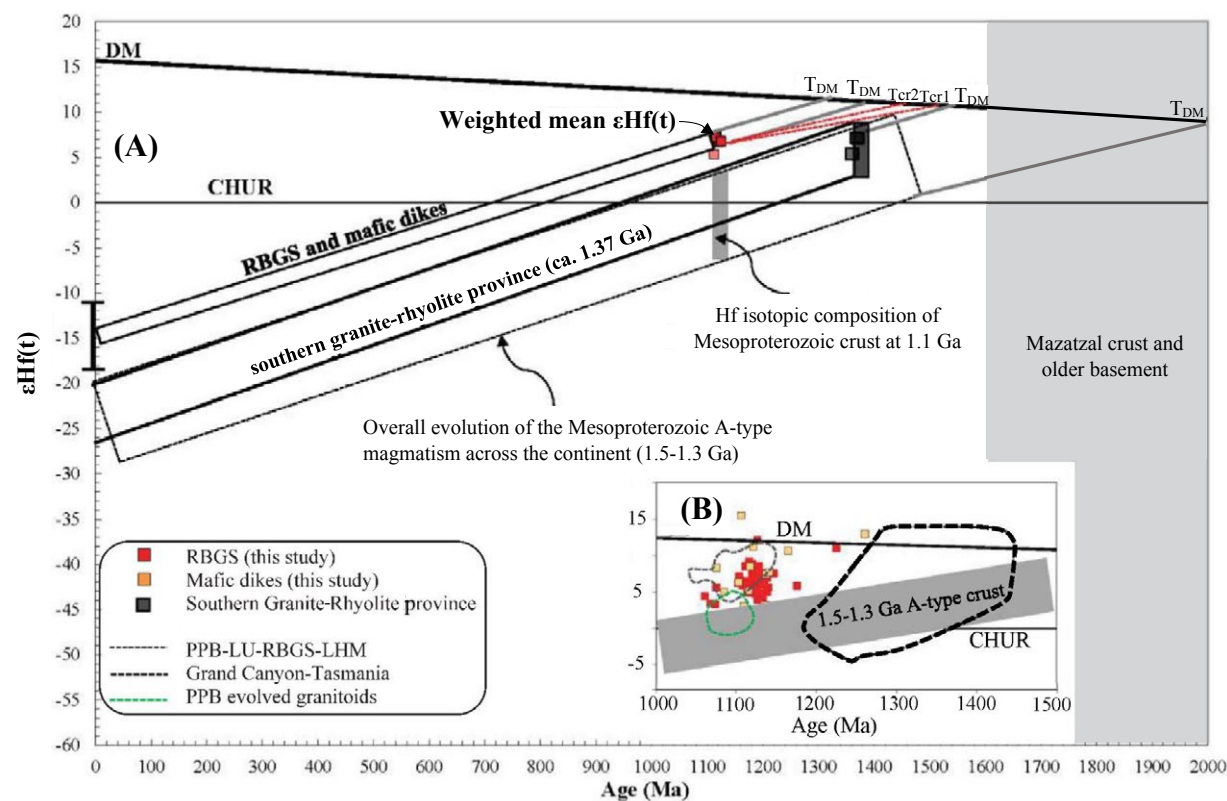


Figure 9. (A) Projected Hf isotopic evolution of Red Bluff Granite Suite (RBGS), mafic dikes, and host Granite-Rhyolite province basement. Single-stage and two-stage (Tcr1 and Tcr2) as well as depleted mantle model ages (T_{DM}) are also shown. The black vertical bar on y-axis shows the overall range of present-day $\epsilon_{\text{Hf}}(t)$ of RBGS. Data for Granite-Rhyolite province are from Goodge and Vervoort (2006) and Bickford et al. (2015). (B) Hafnium isotopic compositions of RBGS along with spatially and temporally related magmatic rocks in southern Laurentian front. Note that Hf isotopic compositions of RBGS are partly comparable to those of Pikes Peak batholith; however, Pikes Peak batholith includes more-evolved [low $\epsilon_{\text{Hf}}(t)$] granitoids. Previous zircon Hf isotopic data are from Guitreau et al. (2016), Hantsche (2015), Howard (2013), and Mulder et al. (2017). PPB—Pikes Peak batholith (Colorado); LU—Llano Uplift (Texas); LHM—Little Hatchet Mountains (New Mexico); DM—depleted mantle; CHUR—chondritic uniform reservoir.

structural settings and overlapping isotopic compositions of RBGS and Llano granitoids suggest tapping of similar sources but in different tectonic settings.

DISCUSSION

Timing of Grenvillian Magmatism as Recorded in West Texas

New LA-MC-ICP-MS U-Pb geochronological data suggest that granitic magmatism in the Franklin Mountains may have been active from 1130 to 1110 Ma.

Therefore, high-precision CA-ID-TIMS U-Pb data are needed to provide robust constraints on the timing of RBGS magmatism. Overlapping crystallization ages for samples FR4 and FR8 from stage 1 and stage 2, respectively, show that the emplacement of these magmatic bodies is tightly restricted at 1112 Ma. Even though cross-cutting relationships indicate that stage 1 syenites are older than the alkali-feldspar granite of stage 2, our ages show that the gap between the initial main two stages is less than one million years. Given lower and upper uncertainties (i.e., 1112.36 \pm 0.35 versus 1112.46 \pm 0.37 Ma), the age gap between stages 1 and 2 may be as much as 0.82 m.y., from 1112.01 to 1112.83 Ma.

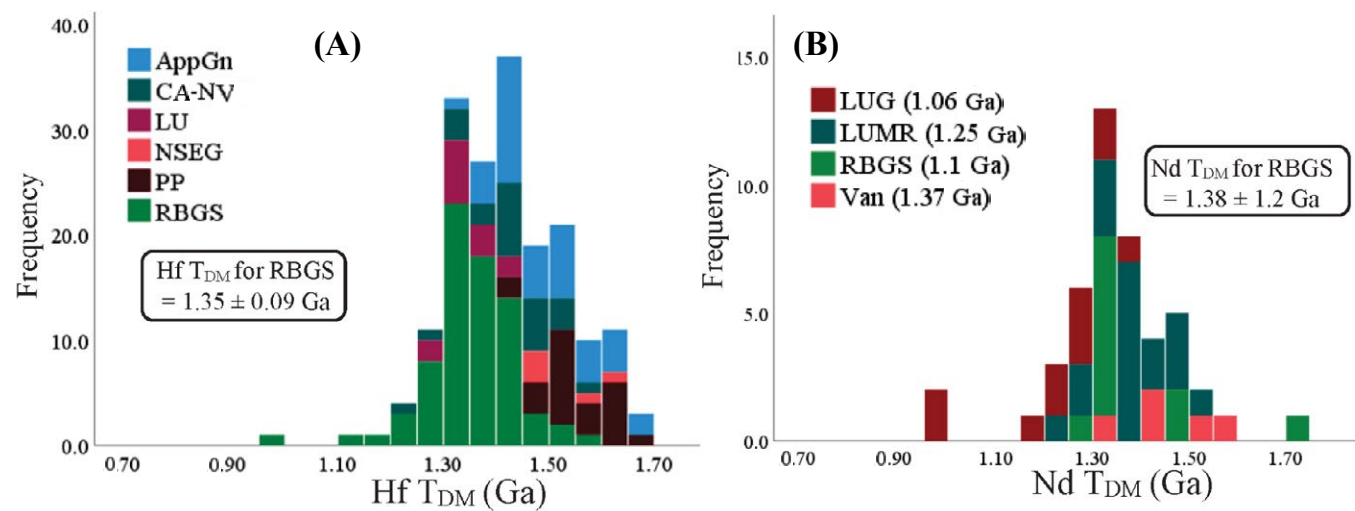


Figure 10. (A) Histogram of single-stage hafnium depleted mantle model ages ($Hf T_{DM}$) of Red Bluff Granite Suite (RBGS) and other 1.1 Ga igneous and metamorphic rocks throughout Grenville Front. Model ages for these 1.1 Ga rocks were calculated by using Hf isotopic data reported by Howard (2013) and in this study. AppGn—Appalachian gneisses; CA-NV—California and southern Nevada; LU—Llano Uplift granitoids; NSEG—northern Sonora (Mexico) Escuadra granites; PP—Pikes Peak batholith (Colorado). (B) Histogram of Nd depleted mantle model ages ($Nd T_{DM}$) of RBGS, Llano area, and Van Horn region rocks from Patchett and Ruiz (1989). Ages shown in parentheses correspond to the timing of emplacement of igneous and metamorphic rocks. LUG—Llano area post-collision granitoids; LUMR—Llano area metamorphic rocks (1.25–1.23 Ga), Van—Van Horn area.

Zircons record inheritance from 1147 to 1313 Ma. Four analyses from the brecciated granitic dike intruding Castner Marble (samples GC1 and GC2) yielded the oldest but variably discordant (12%–18% discordance) dates ranging from 1.36 to 1.30 Ga. Therefore, it can be inferred that the 1112 Ma magmatism might have involved Mesoproterozoic crustal sources. The absence of older zircons (i.e., Mazatzal crust) in west Texas is distinct from the Mazatzal age zircon inheritance within the geochemically similar Mesoproterozoic Pikes Peak batholith, where 1.1 Ga plutons coexist with the earlier Mesoproterozoic epizonal alkalic intrusions (Guitreau et al., 2016). In contrast to data from the RBGS, geochronological data from igneous and metasedimentary rocks in southern New Mexico, located north and northwest of the RBGS, yield ages ranging from 1.68 to 1.62 Ga. These ages indicate that southern New Mexico is part of the Mazatzal crust (Amato et al., 2008, 2011, 2018). Amato et al. (2011, 2018) also provided crystallization ages for the granitoids in southern New Mexico ranging from 1.48 to 1.43 Ga. A similar age range is observed in the detrital zircons from Proterozoic, Ordovician, Devonian, Pennsylvanian, and Cretaceous clastic sedimentary rocks in southern New Mexico (Amato and Mack 2012; Amato, 2019). Zircon inheritance within the ca. 1.1 Ga basaltic dikes has been reported from the Burro Mountains and Antelope Hill in southwestern New Mexico (Fig. 1) (Bright et al., 2014). Both locations fall within the southwestern part of the Mazatzal province (Fig. 1). One inherited zircon

of 1.76 Ga was reported from a basaltic dike exposed in Antelope Hill, and a basaltic dike from the Burro Mountains yielded xenocrystic zircons dated at 2.0–1.4 Ga. However, the RBGS does not show pre-1.37 Ga inheritance, suggesting a minimal contribution from ≥ 1.6 Ga Mazatzal crust.

Dates from younger zircons that are inferred to be xenocrysts range from 1.26 to 1.15 Ga. Similar dates (i.e., ca. 1.15–1.16 Ga) were reported for the Pecos layered mafic and ultramafic rocks of west Texas and New Mexico (Keller et al., 1989). The inherited age of 1.26 Ga is identical to the age of the metatuff embedded within the Castner Marble (Pittenger et al., 1994; Bickford et al., 2000). These dates are similar to those reported for detrital zircons from clastic sedimentary rocks in southern New Mexico (Amato and Mack, 2012) and other Mesoproterozoic basins in the southwestern United States (Mulder et al., 2017) (Fig. 2).

Origin of the RBGS and Other Grenvillian Magmatism in Southwestern Laurentia

Alkaline ferroan magmas high in HFSEs (e.g., Zr, Nb, REEs, Y), $FeO^{total}/(FeO^{total} + MgO)$, and $Na_2O + K_2O - CaO$ and low in trace elements such as Sr, Sc, and Co can be produced by (1) partial melting of quartzo-feldspathic crustal rocks such as tonalitic to grandioritic crust at low pressure; (2) melting and

differentiation of mantle sources, where tholeiitic and alkali-basaltic magmas thus generated undergo differentiation through the processes of fractional crystallization (high pressure) or assimilation–fractional crystallization (low pressure); and (3) variable components of both felsic as well as mafic magmas (e.g., Barker et al., 1975, 1976; Creaser et al., 1991; Foland and Allen, 1991; Turner et al., 1992; Kerr and Fryer, 1993; Frost and Frost, 2011). In the following section, we will discuss the likely source(s) for the RBGS.

Partial Melting of Tonalitic to Granodioritic Crust

Crustal anatexis of rocks with tonalitic compositions was suggested for the geochemically similar potassic and ferroan granites of the Pikes Peak batholith in Colorado (Smith et al., 1999). These granites exhibit comparable major element geochemistry to experimental melt products of tonalitic composition as well as similar Nd isotopic composition to the older tonalitic intrusions in the region. Tonalitic and granodioritic rocks are one of the potential sources; granodioritic orthogneissic xenoliths are reported from the nearby Kilbourne Hole volcanic field in New Mexico (Padovani and Carter, 1977). Also, ca. 1.325–1.275 Ga arc-type rock assemblages were reported from the Cerro Del Carrizalillo and Sierra del Cuervo in northern Mexico (Blount, 1993; Mosher, 1998) and Coal Creek domain in the Llano region (Roback, 1996). Zircon inheritance in the RBGS varying from 1.3 to 1.2 Ga can be related to the partial melting of the tonalitic and granodioritic crust to the south of the RBGS. Among these arc-related assemblages, rocks from Sierra del Cuervo are of particular importance because they lie to the immediate south of west Texas (Fig. 1). The metagabbro and metadiorite of Sierra del Cuervo were emplaced at 1333 ± 10 – 8 Ma and were interpreted to represent the base of a continental margin island arc (Blount, 1993; Mosher, 1998). These rocks, as well as younger calc-alkaline granites within Sierra del Cuervo emplaced at 1274 ± 6 – 5 Ma, are depleted in Y and HREEs. Besides, calculated HFSE and HREE contents generated by the partial-melting modeling of granodiorite and tonalitic sources are lower than those observed in the RBGS (Shannon et al., 1997), and granitic magmas generated by tonalitic melting are commonly magnesian and calc-alkalic to alkalic (Frost et al., 2001). For the RBGS, Shannon et al. (1997) invoked anatexis of an orthopyroxene-rich quartzofeldspathic source, which should be anomalously enriched in U, Th, and HREEs. Therefore, these Y- and REE-depleted tonalitic rocks emplaced at the roots of an arc may not be suitable to generate RBGS source magmas.

Partial Melting of A2-Type Southern Granite-Rhyolite Province Basement

Zircon U–Pb data showing zircon inheritances as old as 1.36 Ga as well as depleted mantle model ages (T_{DM}) (1.4–1.3 Ga) (Figs. 9 and 10) suggest that the source magma might have been generated by the partial melting of Mesoproterozoic basement underneath west Texas. This coupled with overlapping Hf isotopic compositions may indicate that the potassic Granite-Rhyolite province

basement could be a potential source. Magma thus generated would have then mixed with juvenile mantle-derived magmas to produce 1.1 Ga rocks. Alternatively, one can argue that magmas might have been generated from the same sources forming the 1.5–1.3 Ga Granite-Rhyolite basement. Barnes et al. (2002), Goodge and Vervoort (2006), and Bickford et al. (2015) suggested that the Granite-Rhyolite basement was produced by the partial melting of crustal sources older than 1.5 Ga. However, the absence of such older zircon inheritances in RBGS (i.e., >1.36 Ga) as well as younger T_{DM} ages that are primarily restricted between 1.4 and 1.3 Ga (Fig. 10) are not consistent with the partial melting of the protolith of the Granite-Rhyolite basement. Therefore, a simplistic interpretation would be that the RBGS was derived exclusively by melting of alkaline Mesoproterozoic Southern Granite-Rhyolite province (1.38–1.34 Ga) and/or 1.46 Ga crust underneath southern New Mexico and west Texas (e.g., Amato and Mack, 2012; Amato et al., 2018). However, the Southern Granite-Rhyolite province (1.38–1.34 Ga) showed more comparable $\epsilon_{Hf}(t)$ compositions [i.e., $\epsilon_{Hf}(t) = +2.6$ to $+8.9$] (Barnes et al., 2002; Goodge and Vervoort, 2006; Bickford et al., 2015) to those of 1.1 Ga magmatic rocks (Fig. 9).

However, the majority of the ca. 1.37–1.34 Ga granitoids (i.e., Texas Panhandle granitoids and quartz monzonite and syenite) are significantly less enriched in iron with <2 – 3 wt% Fe_2O_3 (Barnes et al., 2002). REE average composition of Southern Granite-Rhyolite basement is also considerably lower than that of the RBGS. Therefore, partial melting of 1.3 Ga granitoids may not have been able to generate source magmas for the RBGS. Also, such anhydrous A-type granitic basement may not have been sufficiently hydrated to facilitate partial melting to generate geochemically similar magmas.

Fractional Crystallization of Mantle-Derived Mafic Magmas

Prolonged fractional crystallization of mafic magma can generate ferroan and alkalic A-type magmas (Frost et al., 2001). Major and trace element chemistry of the RBGS suggests fractionation of feldspars, apatite, ilmenite, and magnetite played an important role.

A Nb/Yb versus Th/Yb plot, modified after Pearce (2008) and Manikyamba and Kerrich (2012), suggests that the dikes are calc-alkaline with enriched mid-ocean-ridge basalt (EMORB) affinities while granitoids dominantly plot at the boundary between the calc-alkaline and shoshonite fields (Fig. 11A). Also, on the Nb/La versus La/Yb and Th/La versus La/Yb discriminant diagrams of Hollocher et al. (2012), mafic samples are borderline continental arc basalts (Figs. 11B and 11C), possibly derived from enriched mantle source(s). Shannon et al. (1997) noticed that these basaltic dikes show a compositional transition from alkaline to subalkaline. Overall, basaltic dikes show enriched trace element characteristics. Th, U, and Hf contents are identical to those of oceanic island basalt (OIB), even though Nb, Ta, and Sr concentrations are lower than those of OIB but are significantly higher than in EMORB (Fig. 11). Lower Nb and Ta concentrations are comparable to those of island arc basalt (Shannon et al., 1997). The basaltic dikes show a weak Eu anomaly with $Eu/Eu^* = 0.9$

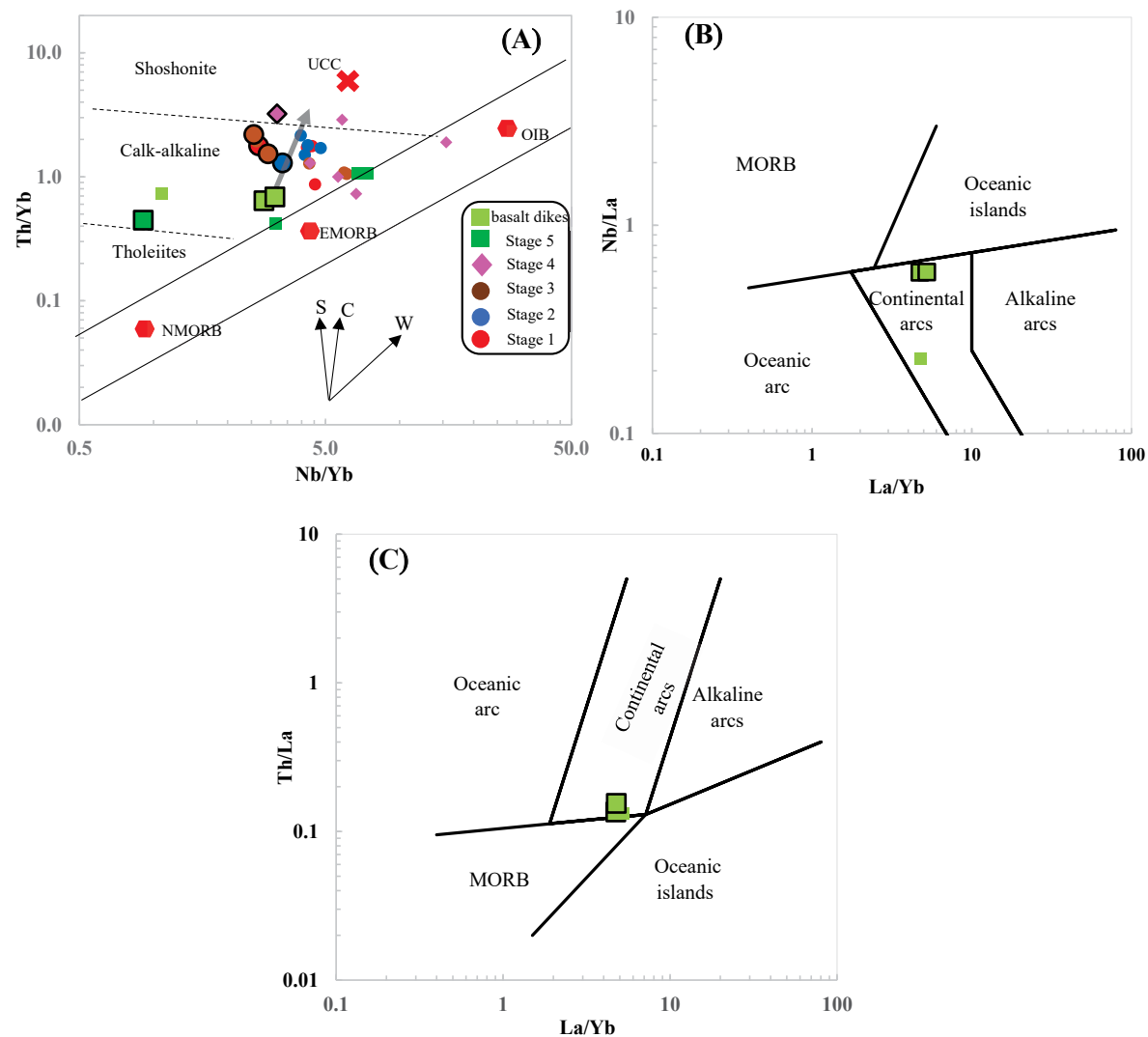


Figure 11. (A) Th/Yb versus Nb/Yb of Red Bluff Granite Suite (RBGS) samples, modified after Pearce (2008) and Manikyamba and Kerrich (2012). Mantle array and average compositions of normal mid-ocean-ridge basalt (NMORB), enriched mid-ocean-ridge basalt (EMORB), and oceanic island basalt (OIB) are shown. UCC—upper continental crust. Thick gray arrow indicates the possible fractionation trend of basaltic magma. Subduction components, crustal contamination, and within-plate evolution are indicated by vectors S, C, and W, respectively. (B and C) Nb/La versus La/Yb and Th/La versus La/Yb discrimination diagrams of Hollocher et al. (2012). Larger symbols with dark borders are from this study.

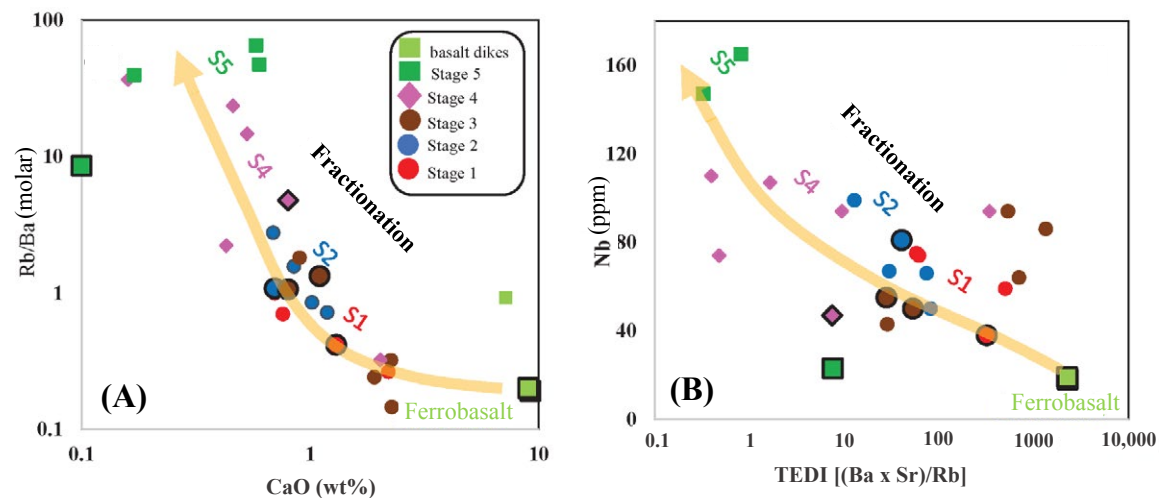


Figure 12. (A) Rb/Ba (molar) versus CaO (wt%) plot of Red Bluff Granite Suite (RBGS) samples suggests dominant role of plagioclase fractionation from parental basaltic magma. (B) Nb versus trace element differentiation index [TEDI; (Ba × Sr)/Rb]. TEDI is from Bailie and Robb (2004). Fractionation trend from ferrobasaltic dikes through different stages of RBGS is also shown. Larger symbols with dark borders are from this study.

(calculated using the geometric mean [Eu anomaly, Eu/Eu^* is calculated as: $Eu_N / (Sm_N \times Gd_N)^{1/2}$, N represents chondrite normalization of Eu, Sm, and Gd.]). Enrichment in Rb, Ba, Zr, and REEs as compared to OIB (Fig. 6) indicates crustal contamination or derivation of basaltic dikes from enriched mantle sources such as subcontinental lithospheric mantle.

The above discussion suggests that both the basalts and granitic rocks are derived from enriched magma sources. One can hypothesize that the RBGS and associated mafic dikes are consanguineous and produced from the same magma source, where basaltic dikes are the offshoots of a parent basaltic magma at depth and the RBGS was produced by the differentiation of such magma.

We now test whether the RBGS could have been produced by the differentiation of basalt compositionally similar to the spatially and temporally related ferrobasaltic dikes. Large-ion lithophile elements are sensitive to the magmatic evolution process; an increase of Rb/Ba and Rb/Sr ratios is indicative of fractionation of plagioclase. A plot of Rb/Ba (molar) versus CaO (wt%) (Fig. 12A) indicates that the various granite facies of the RBGS resulted from the fractionation of a parental ferrobasaltic source. The trace element discrimination index (TEDI), defined as $(Ba \times Sr)/Rb$ (Bailie and Robb, 2004), has been successfully used to identify petrogenetic processes like fractional crystallization; a decrease in TEDI suggests an increase in magma fractionation. It is particularly helpful for evaluating whether the various granitic rocks within an igneous suite are genetically related and result from the progressive fractionation of an initial granitic magma (e.g., Vonopartis et al., 2020; Gardiner et al., 2021). An Nb versus TEDI plot suggests that the RBGS was derived from a ferrobasaltic source (Fig. 12B).

On the basis of the observed geochemical characteristics, fractional crystallization (FC) processes involving ferrobasaltic magma appear to be the potential mechanism for generation of the RBGS. To provide further constraints for this interpretation, we performed trace element modeling for FC and/or assimilation-fractional crystallization (AFC) of such basaltic source(s). We carried out both FC-only runs and AFC runs using FC-AFC-FCA (decoupled assimilation and fractional crystallization) and the mixing modeler program of Ersoy and Helvacı (2010). For the parental melt composition, we tested both mafic dikes within the RBGS as well as Mesoproterozoic gabbroic sills in west Texas (Barnes et al., 2002). Both basaltic dike samples (LAM2 and LAM3) and gabbroic sills show comparable Al_2O_3 , Na_2O , and P_2O_5 contents. However, basaltic dikes show a higher CaO content of 9.2 wt% and gabbro showed an elevated MgO content of 8.2 wt%. Gabbroic sills show lower contents for Zr and Nb as compared to the basaltic dikes. The Gabbroic sills show a higher SiO_2 content of 49.8 wt%. For FC, basaltic dikes approximate the initial source composition for the RBGS, even though gabbroic sills also generated comparable results. For the AFC modeling, the composition of the lower continental crust (Taylor and McLennan, 1995) is used as the potential assimilate. The observed REE data trend for RBGS is consistent with both the FC and AFC modeled trends, showing overlapping steeper LREE and flat HREE patterns (Fig. 13A). However, the FC and AFC models for the initial composition of sample LAM2 did not yield the strong negative anomalies of Ti, Ba, and Eu observed in the RBGS. We obtained the best fit for FC and AFC models using the values of these three elements lower than the LAM2 (e.g., 1 wt%, 300 ppm, and 2 ppm, respectively) (Figs. 13A and

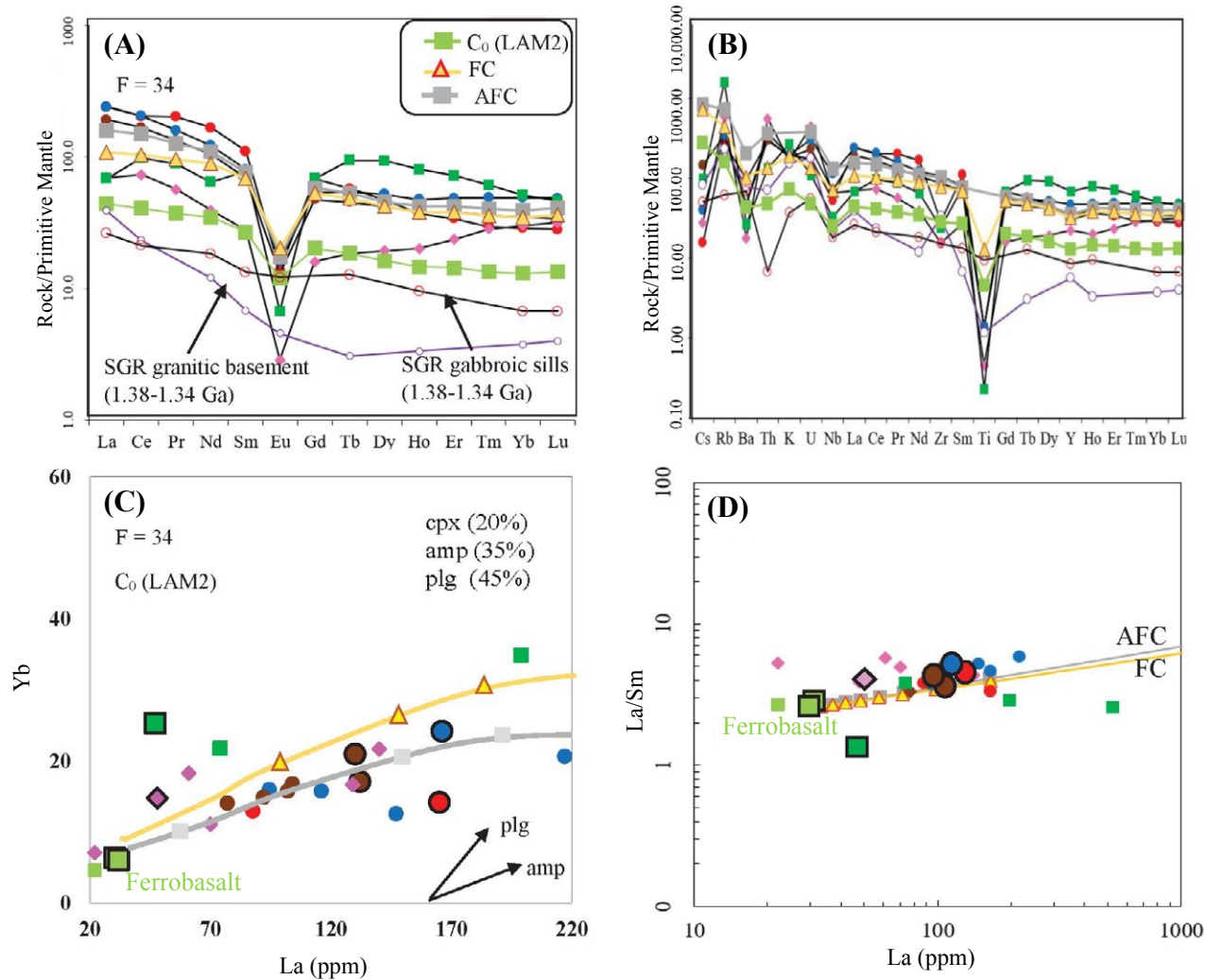


Figure 13. (A and B) Primitive mantle (PM)-normalized rare earth element (REE) (A) and trace element (B) spider diagrams for representative samples from Red Bluff Granite Suite (RBGS); average composition of 1.38–1.34 Ga granitoids and gabbroic sills (i.e., southern Granite-Rhyolite province) underneath west Texas are from Barnes et al. (2002). Mesoproterozoic granitoids underneath are significantly depleted in REEs, and therefore should not be considered as one of the dominant sources producing RBGS. Modeling results for fractional crystallization (FC) and assimilation–fractional crystallization (AFC) are shown. Slightly modified composition (C₀) (see discussion in text) of ferrobasaltic dike (sample LAM2) is used to approximate parental basaltic magma composition for RBGS (see text). For AFC, lower continental crust (Taylor and McLennan, 1995) is used as the assimilant. (C) Yb versus La plot showing modeling curves for FC and AFC processes. FC-AFC modeling was performed using FC-AFC-FCA (decoupled assimilation and fractional crystallization) and mixing modeler program of Ersoy and Helvacı (2010). Arrows labelled with plg and amp indicate fractionation trend of plagioclase and amphibole. SGR—Southern Granite-Rhyolite province; cpx—clinopyroxene. (D and E) La/Sm versus La (D) and Zr/Nb versus Zr (E) diagrams clearly showing that fractional crystallization remained a dominant process at ca. 1.1 Ga; slight increase in elemental ratio such as Zr/Nb indicates some contribution of partial melting of crustal sources. Larger symbols with dark borders are from this study. F—melt fraction. (Continued on following page.)

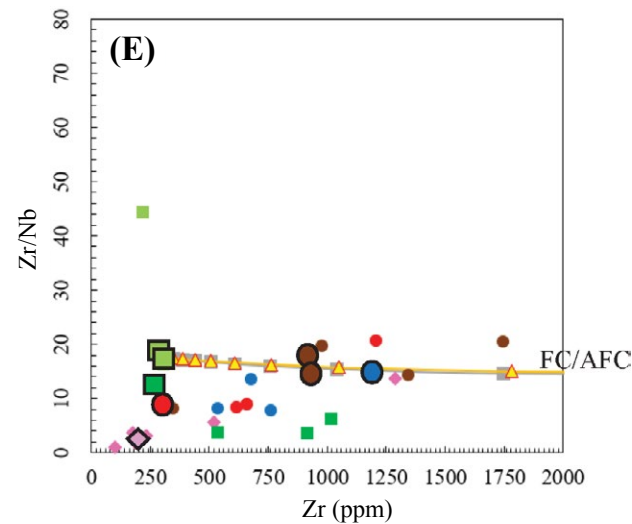


Figure 13 (Continued).

13B). This suggests that the RBGS is derived from fractional crystallization of a basaltic source with a minor contribution from the crustal melt.

Modeling results suggest that the RBGS represents fractionated melt derived through significant fractionation of plagioclase, clinopyroxene, and amphibole from mildly evolved parental, mantle-derived ferrobasic magmas that were compositionally similar to the coeval basaltic dikes (Figs. 13A and 13B). A Yb versus La plot suggests that FC and AFC are the likely processes in which plagioclase, pyroxene, and amphibole are the main fractionation phases (Fig. 13C). The ratios of incompatible elements do not significantly change during fractional crystallization, and therefore plots of the ratio of a highly incompatible element to a less-incompatible element versus highly incompatible element would produce a less steep slope. On the other hand, the partial melting of crustal sources would considerably increase the concentration of highly incompatible elements, giving a much steeper slope and linear trend. Therefore, such plots are meant to differentiate the partial melting and fractional crystallization processes. Plots of La/Sm versus La and Zr/Nb versus Zr show a clear trend suggesting that the source magma was controlled by fractional crystallization with a minor contribution of crustal melt (Figs. 13D and 13E). Figures 12 and 13 show the magma evolution pathway suggesting fractionation of basaltic source can generate an initial alkali-feldspar quartz syenite and/or syenogranite (stage 1 of the RBGS) which through progressive fractionation would have evolved to stage 2 alkali-feldspar granite. Stages 2, 4, and 5 can be explained by the progressive fractionation of the granitic melt. However, stage 3 biotite–amphibole–alkali feldspar quartz syenite does not show a conclusive derivation from stage 2. This discrepancy was also noted

by Shannon et al. (1997). Based on geochemical data, they suggested that it is likely that the stage 3 syenite is directly derived from ferrobasic magmas.

From the above discussion, it is evident that the RBGS mafic as well as granitic rocks were likely produced by the differentiation of mantle-derived mafic magmas through FC and/or AFC processes with some assimilation from crust as evident by older zircon inheritances. However, this interpretation is plagued by the much older 1.4–1.3 Ga Hf and Nd depleted mantle model ages (T_{DM}) (Fig. 10). These T_{DM} ages are 300–250 m.y. older than the crystallization ages of the RBGS and call into question the direct involvement of mantle-derived magma. Also, trace element geochemistry (i.e., enriched REE pattern) and enriched Hf isotopic composition [$\epsilon_{Hf}(t) = +5$ to $+7$] are not consistent with significant contribution from sublithospheric mantle (depleted mantle), given that depleted mantle would have had an $\epsilon_{Hf}(t)$ value of $\sim +12$ at 1.1 Ga (Vervoort and Blichert-Toft, 1999). This leads to a fundamental question: When and where were the 1.1 Ga magmas produced?

Hafnium and Nd model ages are considered to represent the time when the new continental crust was extracted from the depleted mantle and may serve as the ceiling of radiogenic signatures. This assumes that the isotopic composition of the depleted mantle is comparable to that of the juvenile crust at the time it is derived from the mantle. However, on the basis of enriched Hf isotopic compositions [i.e., $\epsilon_{Hf}(t)$ below the depleted mantle curve] of island arcs as compared to the depleted mantle (i.e., new continental crust), Dhuime et al. (2011) suggested that the model ages of the isotopically enriched new crust should not be calculated from the composition of the depleted mantle and that such model ages should correspond to an isotopically enriched material representing new continental crust at the time of its derivation from the mantle source. That means the depleted mantle should not be treated as the only possible reservoir from which mantle melting can occur to generate juvenile continental crust (Vervoort and Kemp, 2016; Spencer et al., 2020). This also implies that T_{DM} ages are not an accurate measure of the timing of when the melting occurred. Dhuime et al. (2011) proposed an additional isotopic reservoir from which mantle melts can be derived that has a lower $\epsilon_{Hf}(t)$ than the depleted mantle. Dhuime et al. (2011) named this new mantle reservoir as “new crust” and the model ages calculated from the new crust are ~ 300 m.y. younger than the T_{DM} ages. Also, this new continental crust has a present-day Hf isotopic composition of $+13.2 \pm 1.1$, which is considerably more enriched than the depleted mantle [i.e., $\epsilon_{Hf}(0) = +15$]. Such a mantle would have a Hf isotopic composition lower than that of the depleted mantle.

Derivation from an enriched mantle source might be the case for the origin of the RBGS as well as other 1.1 Ga granitoids in southwestern Laurentia. Particularly, the RBGS which was produced by the fractional crystallization of an enriched mantle-derived magma, is having lower $\epsilon_{Hf}(t)$ than the depleted mantle. The new crust (NC) model ages [i.e., $age_{(NC)} = age_{(DM)} - 0.3$ Ga] of magmatic rocks in southwestern Laurentia largely overlap with the crystallization ages (Fig. 14A). Particularly, the RBGS and Llano Uplift rocks yielded an average new crust model age of 1.08 ± 0.05 Ga. However, the Pikes Peak batholith and Appalachian gneisses yielded older new crust model ages of

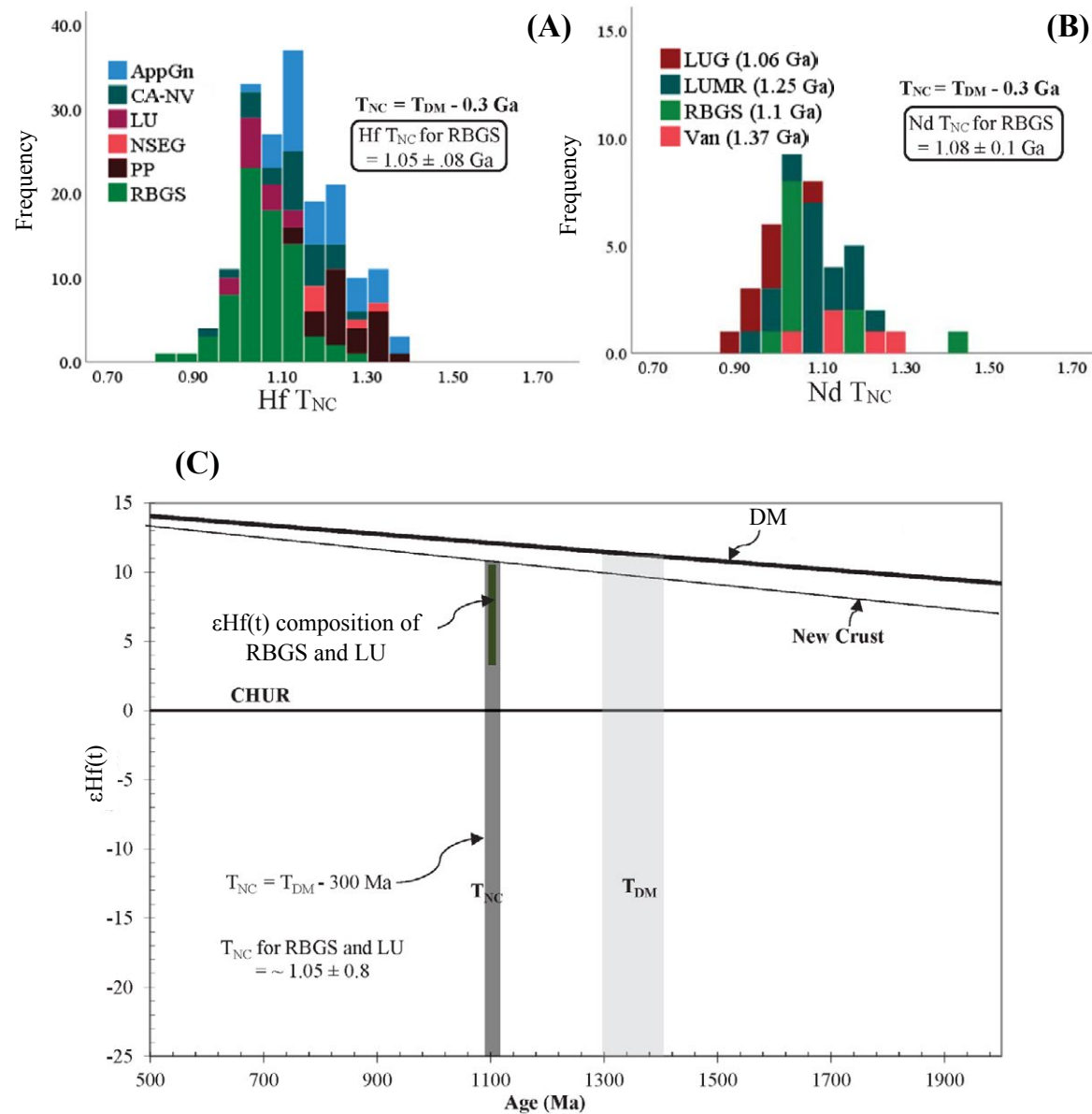


Figure 14. (A and B) Histogram of model ages calculated for new crust ($T_{NC} = T_{DM} - 0.3 \text{ Ga}$, where T_{DM} is depleted mantle model age) after Dhuime et al. (2011). (C) Hf isotopic evolution of 1.1 Ga magmatic rocks of southwestern Laurentia for depleted and enriched new continental crustal reservoir. CHUR—chondritic uniform reservoir. Symbols, other abbreviations, and data sources are same as in Figure 10.

1.25 and 1.18 Ga, respectively. Similar to Hf isotopic data, we suggest that the new crust Nd model ages are appropriate for the crust with enriched Nd isotopic composition of $\epsilon\text{Nd}(t) = +2.5$ to $+5$. The new crust Nd model ages show a near-complete overlap with the crystallization ages of RBGS and Llano Uplift granitoids (Fig. 14B). Figure 14C is the graphical representation of the depleted mantle and new crust model ages. A similar problem was discussed by Bickford et al. (2010) for Adirondack AMCG (anorthosite-mangerite-charnockite-granite) suites (New York, USA), where enriched granite-anorthosites yielded depleted mantle model ages 200–150 m.y. older than the crystallization ages while petrological data support partial melting of pre-existing enriched crust or mantle lithosphere or mixing of both. They interpreted that these granites and anorthosites were derived from a distinct enriched mantle reservoir through processes of FC and AFC; perhaps it is similar to the enriched mantle material named as new crust by Dhuime et al. (2011).

Therefore, petrological data supportive of fractional crystallization coupled with enriched $\epsilon\text{Hf}(t)$ values lower than those of the depleted mantle provide useful support for a diverse array of isotopic reservoirs from which mantle melting occurred. This implies that such an enriched mantle reservoir was produced during the preceding arc-related magmatic activities in southwestern Laurentia ca. 1.3–1.25 Ga, where older Hf might have recycled from the preceding subducted lithosphere resulting in younger model ages (Vervoort

and Kemp, 2016). A similar origin is suggested for the Adirondack AMCG suites (Bickford et al., 2010).

Tectonic Implications

On the basis of detrital zircon geochronological and Hf isotopic data from sediments in the Grand Canyon, Arizona, USA, and Tasmania, southeast Australia, Mulder et al. (2017, 2018) placed Tasmania as well as Kalahari (southern continental block) adjacent to southwestern Laurentia in the late Mesoproterozoic ca. 1.14–0.9 Ga (Figs. 9 and 15). Initially, the southwestern Laurentian margin evolved as a Himalayan-type convergent margin, where a southern slab subducted beneath the Laurentian margin and an arc accreted to the southern margin of Laurentia ca. 1250–1230 Ma. This is coeval with the development of an orogen-parallel backarc basin and deposition of carbonate and siliciclastic deposits above a Mesoproterozoic basement (Fig. 16A). In the Van Horn area of west Texas, the Millican Hills are overthrust by 1.38–1.33 Ga bimodal metavolcanic and metasedimentary rocks and gabbro-diorite plutons of the Carrizo Mountain Group (Bickford et al., 2000; Davis and Mosher, 2015). On the basis of geochemical data, Rudnick (1983) and Roths (1993) suggested that the Carrizo Mountain Group accumulated in a backarc basin.

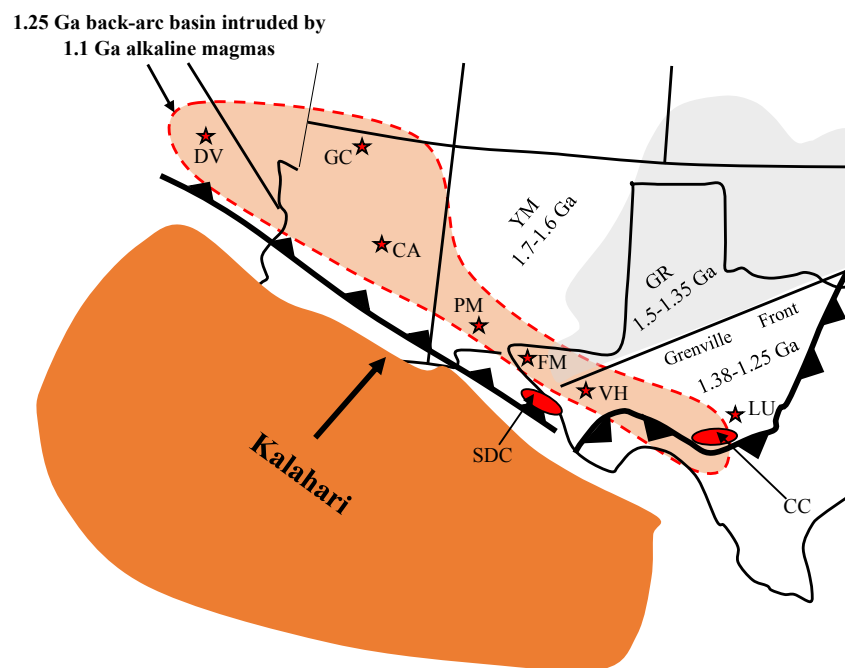
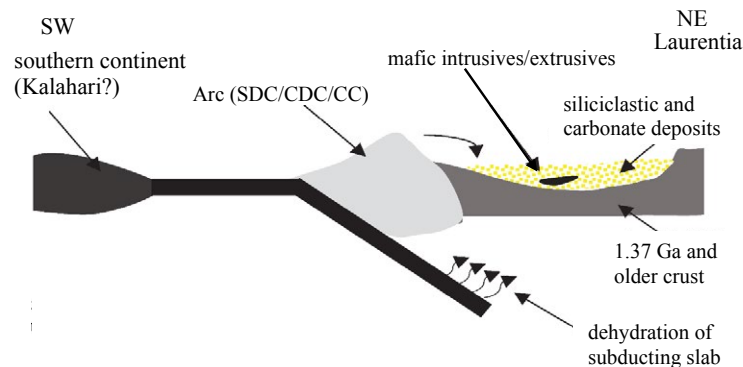
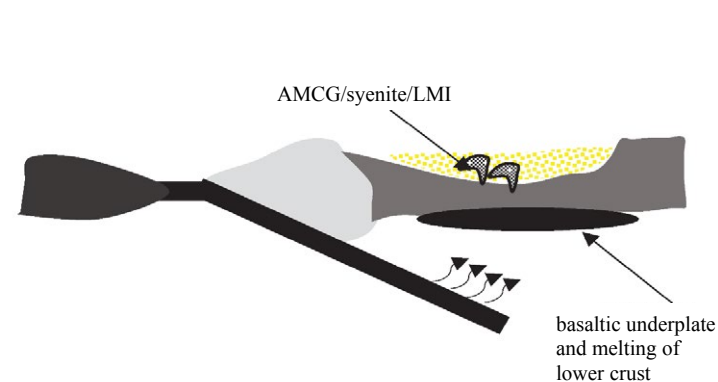


Figure 15. Proposed paleogeographic reconstruction of southwestern Laurentia at ca. 1.1 Ga to 0.90 Ga, modified after Merdith et al. (2017) and Mulder et al. (2018), involving continent-continent collision with continental block (Kalahari) lying to southwest of Laurentia. Coal Creek domain (CC) and Sierra del Cuervo (SDC) represent remnants of arc emplaced at ca. 1.325–1.275 Ga (see text for discussion). Locations of ca. 1.1 Ga magmatism within northwest-striking 1.25 Ga sedimentary basins and structural elements are modified after Bickford et al. (2000) and Timmons et al. (2005). GR—Granite-Rhyolite province; LU—Llano; VH—Van Horn; FM—Franklin Mountains; PM—Pajarito Mountain, New Mexico; CA—south-central Arizona; GC—Grand Canyon; DV—Death Valley, California. YM—Yavapai and Mazatzal provinces.

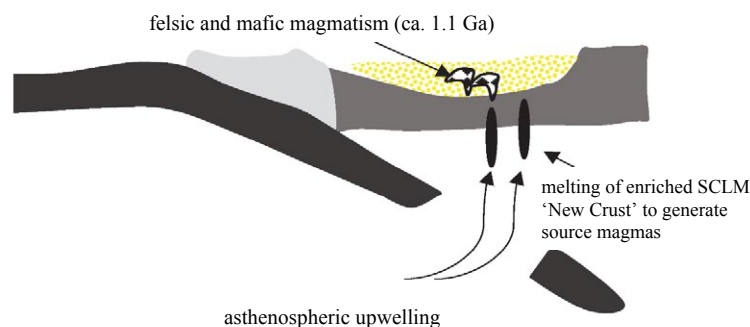
A) Continent-arc-type Laurentian margin (1250-1230 Ma)



B) Basaltic underplate and associated magmatism (1230-1150 Ma)



C) Himalayan-type collision and slab breakoff (1140-1100 Ma)



D) Continent-continent collision, subduction reversal and south-dipping thrusting (1100-980 Ma)

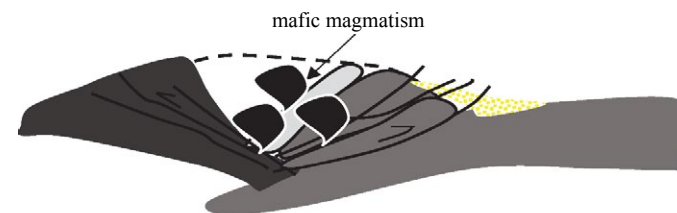


Figure 16. Schematic tectonic evolution of southwestern Laurentian margin and associated magmatism. (A) Southwestern Laurentia remained continent-arc-type margin, with northeastward subduction of southern slab, resulting in backarc basin development from 1250 to 1230 Ma. Gabbroic sills of west Texas (Barnes et al., 2002), Coal Creek domain arc of the Llano area, Texas (CC), and metagabbro of Sierra del Cuervo (SDC) as well as tonalite, trondhjemite, and granite dikes of Cerro Del Carrizalillo (CDC) of northern Mexico (Blount, 1993; Mosher, 1998) can be attributed to subduction-related magmatism during the Mesoproterozoic (1.38–1.34 Ga). (B) Northward subduction continued from 1230 to 1150 Ma resulting in generation of felsic as well as mafic magmas as evident by AMCG (anorthosite-mangerite-charnockite-granite) suites of California, alkaline magmatic rocks in New Mexico, layered mafic intrusions (LMI) of Texas, and detrital zircon data across southwestern Laurentia. (C) Himalayan-type collision and slab break-off of southern continent underneath southwestern Laurentia from 1140 to 1100 Ma. Asthenospheric upwelling through slab window facilitated partial melting of enriched subcontinental lithospheric mantle (SCLM) to generate ferrobasaltic magma, which, upon fractional crystallization, resulted in emplacement of 1.1 Ga ferroan and alkaline granites within 1.25 Ga Mesoproterozoic sedimentary sequences. (D) Subduction zone reversal, south-dipping thrusting, post-collisional magmatism, uplift in the Llano region, and mafic magmatism throughout southwestern Laurentia from 1100 to 980 Ma.

Bickford et al. (2000) suggested that the Carrizo Mountains mark the southernmost exposures of the Southern Granite Rhyolite province (ca. 1.37 Ga). This observation is consistent with the presence of zircon inheritance of ca. 1.3 Ga within the 1.1 Ga granitoids. Calc-alkaline rock assemblages of Cerro Del Carrizalillo and Sierra del Cuervo in northern Mexico (Blount, 1993; Mosher, 1998) and the Coal Creek domain in the Llano Uplift (Roback 1996) emplaced at ca. 1.325–1.275 Ga are likely the remnants of the arc (Mosher, 1998; Davis and Mosher, 2015) (Fig. 16A). Particularly, Sierra del Cuervo is emplaced south of west Texas (Mosher, 1998). However, Mosher (1998) related the collision of the arc to southern Laurentia between 1150 and 1120 Ma during the collision of the southern continent to Laurentia. Based on the lack of subduction-related magmatic activity in the Llano area during 1232–1120 Ma (see Fig. 2), Mosher (1998) and Mosher et al. (2008) suggested that the northward subduction of the southern continent was terminated between 1232 Ma and 1150 Ma in the Llano Uplift. Mosher (1998) speculated that the northward subduction zone might have reversed when the southern continent arrived at the subduction zone in west Texas. Subsequent convergence had a southward polarity, which finally led to the continent-continent collision and slab failure (i.e., slab break-off) of the Laurentian slab (Mosher, 1998; Mosher et al., 2008). This finally resulted in asthenospheric upwelling, basaltic underplating, partial melting of the lower crust, and juvenile granitic magma intrusion (Mosher et al., 2008). However, Mulder et al. (2017), on the basis of the 1.2–1.18 Ga AMCG suite of California, suggested continued northward subduction until 1.18 Ga (Fig. 16B). Mulder et al. (2017) also reported the dominant age peaks of this period from the Hazel Formation (1205 Ma), Dox Formation (1201 Ma), and Shinumo Sandstone (1184 Ma). They attributed the origin of these zircons to the once-existing post-orogenic magmatic rocks within southwestern Laurentia. We suggest that the magmatic rocks of the Pecos layered mafic and ultramafic rocks emplaced at ca. 1.15 Ga in west Texas and New Mexico (Keller et al., 1989), 1.17 Ga syenites of Pajarito Mountain in New Mexico (Kelley, 1968), 1.2–1.18 Ga AMCG suites of Eagle and San Gabriel in California (Barth et al., 2001; Wooden et al., 2013), and inherited zircons in the RBGS (1.2–1.15 Ga) (this study) are indicative of the continued northward subduction-related igneous activity during 1.2–1.15 Ga (Figs. 15 and 16B). This suggests that following ca. 1232 Ma, the cessation of magmatism during ca. 1230–1120 Ma interpreted for the Llano region (Mosher, 1998) may not be supported for west Texas and further to the northwest.

During 1140–1120 Ma, ongoing convergence resulted in a Himalayan-type collision of the southern continent to the arc and subduction of the southern slab underneath the Laurentian margin (Fig. 16C). Break-off of this southern slab underneath the Laurentian margin facilitated asthenospheric upwelling and induced partial melting of an enriched mantle reservoir, possibly subcontinental lithospheric mantle. Differentiation of such magmas through extensive FC and/or AFC processes resulted in the emplacement of 1.1 Ga granitoids within the carbonate and siliciclastic deposits (Fig. 16C). In west Texas, at ca. 1.1 Ga, felsic magma intruded the temporally and spatially correlated Allamoore-Tumbledown Formations of the Millican Hills in the Van Horn area and the Castner Marble–Mundy Breccia in the Franklin Mountains. Finally, ca.

1060 Ma, the subduction zone reversal resulted in the south-dipping thrusts and intrusion of younger mafic intrusions (Fig. 16D).

CONCLUSIONS

- (1) Zircon U-Pb dating on zircons from the Red Bluff Granite Suite assigned a range of crystallization ages from 1112.01 to 1112.83 Ma for the earliest two magmatic stages.
- (2) Whole-rock geochemistry and petrological data are supportive of fractional crystallization of a ferrobasaltic magma compositionally similar to the associated basaltic dikes. This, tied to the enriched Hf isotopic compositions, suggests the melting of an enriched mantle reservoir. Given the zircon inheritance of ca. 1.3 Ga, a minor contribution from the Mesoproterozoic felsic crust cannot be ruled out.
- (3) We suggest that the basaltic dikes and felsic magmatic rocks are consanguineous and produced by the partial melting of the same enriched mantle source. The Proterozoic magmatism in the Franklin Mountains and Llano Uplift as well as other 1.1 Ga intrusions within the northwestward-directed Mesoproterozoic (1.25 Ga) orogen-parallel sedimentary basins require convergence of a continental block to the southwest of the Laurentian margin.
- (4) We propose that 1.1 Ga ferroan A2-type granitic source magmas were produced dominantly by partial melting of an enriched mantle reservoir, possibly subcontinental lithospheric mantle. Partial melting was facilitated by asthenospheric upwelling during a post-collisional slab break-off event underneath the southern margin of Laurentia.

ACKNOWLEDGMENTS

We are grateful to Mark Pecha at the Arizona LaserChron Center, University of Arizona, for technical assistance with sample preparation, analysis, acquisition of geochronological and Hf isotopic data, reduction of isotopic data (U-Pb and Hf), and zircon cathodoluminescence imaging. This manuscript benefited from thoughtful reviews by R.S. Hildebrand, J.B. Whalen, J.M. Amato, S. Mosher, and an anonymous reviewer for which the authors are grateful; we greatly appreciate their valuable feedback. We also thank M.E. Bickford for thoughtful discussions about the Grenville tectonic evolution and implications of the Hf isotopic data.

REFERENCES CITED

- Adams, D.C., and Keller, G.R., 1994, Possible extension of the Midcontinent Rift in west Texas and eastern New Mexico: *Canadian Journal of Earth Sciences*, v. 31, p. 709–720, <https://doi.org/10.1139/e94-063>.
- Amarante, J.F.A., Kelley, S.A., Heizler, M.T., Barnes, M.A., Miller, K.C., and Anthony, E.Y., 2005, Characterization and age of the Mesoproterozoic Debaca sequence in the Tucumcari Basin, New Mexico, in Karlstrom, K.E., and Keller, G.R., eds., *The Rocky Mountain Region: An Evolving Lithosphere: American Geophysical Union Geophysical Monograph* 154, p. 185–199, <https://doi.org/10.1029/154GM13>.
- Amato, J.M., 2019, Detrital zircon ages from Proterozoic, Paleozoic, and Cretaceous clastic strata in southern New Mexico: *Rocky Mountain Geology*, v. 54, p. 19–32, <https://doi.org/10.24872/rmgjournal.54.1.19>.
- Amato, J.M., and Mack, G.H., 2012, Detrital zircon geochronology from the Cambrian–Ordovician Bliss Sandstone, New Mexico: Evidence for contrasting Grenville-age and Cambrian sources

- on opposite sides of the Transcontinental Arch: Geological Society of America Bulletin, v. 124, p. 1826–1840, <https://doi.org/10.1130/B306571>.
- Amato, J.M., Boullion, A.O., and Sanders, A.E., 2008, Magmatism and metamorphism at 1.46 Ga in the Burro Mountains, southwestern New Mexico, *in* Mack, G., Witcher, J., and Lueth, V.W., eds., *Geology of the Gila Wilderness–Silver City Area: New Mexico Geological Society 59th Annual Fall Field Conference Guidebook*, p. 107–115, <https://doi.org/10.56577/FFC-59.107>.
- Amato, J.M., Heizler, M.T., Boullion, A.O., Sanders, A.E., McLemore, V.T., Toro, J., and Andronicos, C.L., 2011, Syntectonic 1.46 Ga magmatism and rapid cooling of a gneiss dome in the southern Mazatzal Province: Burro Mountains, New Mexico: Geological Society of America Bulletin, v. 123, p. 1720–1744, <https://doi.org/10.1130/B303371>.
- Amato, J.M., Ottenfeld, C.F., and Howland, C.R., 2018, U–Pb geochronology of Proterozoic igneous and metasedimentary rocks in southern New Mexico: Post-collisional S-type granite magmatism, *in* Mack, G.H., Hampton, B.A., Ramos, F.C., Witcher, J.C., and Ulmer-Scholle, D.S., eds., *Las Cruces Country III: New Mexico Geological Society 69th Annual Fall Field Conference Guidebook*, p. 137–145, <https://doi.org/10.56577/FFC-69.137>.
- Andersen, T., Griffin, W.L., and Pearson, N.J., 2002, Crustal evolution in the SW part of the Baltic Shield: The Hf isotope evidence: *Journal of Petrology*, v. 43, p. 1725–1747, <https://doi.org/10.1093/petrology/43.9.1725>.
- Anthony, E.Y., Barnes, C.G., Chen, W., Hoffer, J.M., Keller, G.R., Marsaglia, K.M., McLemore, V.T., Seeley, J.M., Seward, M.A., Shannon, W.M., and Thomann, W.F., 1991, Examples of modern rift volcanism and Proterozoic anorogenic magmatism: The Potrillo volcanic field of southern New Mexico and the Franklin Mountains of west Texas, *in* Julian, B., and Zidek, J., eds., *Field Guide to Geologic Excursions in New Mexico and Adjacent Areas of Texas and Colorado: New Mexico Bureau of Mines and Mineral Resources Bulletin 137*, p. 1–3.
- Bailie, R.H., and Robb, L.J., 2004, Polymetallic mineralization in the granites of the Bushveld complex: Examples from the central southeastern lobe: *South African Journal of Geology*, v. 107, p. 633–652, <https://doi.org/10.2113/gssajg.107.4.633>.
- Barker, F., Wones, D.R., Sharp, W.N., and Desborough, G.A., 1975, The Pikes Peak batholith, Colorado Front Range, and a model for the origin of the gabbro–anorthosite–syenite–potassic granite suite: *Precambrian Research*, v. 2, p. 97–160, [https://doi.org/10.1016/0301-9268\(75\)90001-7](https://doi.org/10.1016/0301-9268(75)90001-7).
- Barker, F., Hedge, C.E., Millard, H.T., O’Neil, J.R., Epis, R.C., and Weimer, R.J., 1976, Pikes Peak batholith: Geochemistry of some minor elements and isotopes, and implications for magma genesis: *Professional Contributions of Colorado School of Mines: Studies in Colorado Field Geology*, v. 8, p. 44–56.
- Barnes, C.G., Shannon, W.M., and Kargi, H., 1999, Diverse Mesoproterozoic basaltic magmatism in west Texas: *Rocky Mountain Geology*, v. 34, p. 263–273, <https://doi.org/10.2113/34.2.263>.
- Barnes, M.A., Anthony, E.Y., Williams, I., and Asquith, G.B., 2002, Architecture of a 1.38–1.34 Ga granite–rhyolite complex as revealed by geochronology and isotopic and elemental geochemistry of subsurface samples from west Texas, USA: *Precambrian Research*, v. 119, p. 9–43, [https://doi.org/10.1016/S0301-9268\(02\)00116-X](https://doi.org/10.1016/S0301-9268(02)00116-X).
- Barth, A.P., Wooden, J.L., and Coleman, D.S., 2001, SHRIMP-RG U–Pb zircon geochronology of Mesoproterozoic metamorphism and plutonism in the southwesternmost United States: *The Journal of Geology*, v. 109, p. 319–327, <https://doi.org/10.1086/319975>.
- Bickford, M.E., Soegaard, K., Nielsen, K.C., and McLelland, J.M., 2000, Geology and geochronology of Grenville-age rocks in the Van Horn and Franklin Mountains area, west Texas: Implications for the tectonic evolution of Laurentia during the Grenville: *Geological Society of America Bulletin*, v. 112, p. 1134–1148, [https://doi.org/10.1130/0016-7606\(2000\)112<1134:GAGOGR>2.0.CO;2](https://doi.org/10.1130/0016-7606(2000)112<1134:GAGOGR>2.0.CO;2).
- Bickford, M.E., McLelland, J.M., Mueller, P.A., Kamenov, G.D., and Neadle, M., 2010, Hafnium isotopic compositions of zircon from Adirondack AMCG suites: Implications for the petrogenesis of anorthosites, gabbros, and granitic members of the suites. *The Canadian Mineralogist*, v. 48, p. 751–761, <https://doi.org/10.3749/canmin.48.2.751>.
- Bickford, M.E., Van Schmus, W.R., Karlstrom, K.E., Mueller, P.A., and Kamenov, G.D., 2015, Mesoproterozoic–trans-Laurentian magmatism: A synthesis of continent-wide age distributions, new SIMS U–Pb ages, zircon saturation temperatures, and Hf and Nd isotopic compositions: *Precambrian Research*, v. 265, p. 286–312, <https://doi.org/10.1016/j.precamres.2014.11.024>.
- Blount, J.G., 1993, The geochemistry, petrogenesis, and geochronology of the Precambrian meta-igneous rocks of Sierra Del Cuervo and Cerro El Carrizalillo, Chihuahua, Mexico [Ph.D. thesis]: Austin, University of Texas, 242 p.
- Bright, R.M., Amato, J.M., Denyszyn, S.W., and Ernst, R.E., 2014, U–Pb geochronology of 1.1 Ga basaltic in the southwestern United States: Testing models for the origin of a post-Grenville large igneous province: *Lithosphere*, v. 6, p. 135–156, <https://doi.org/10.1130/L1335.1>.
- Cecil, M.R., Gehrels, G., Ducea, M.N., and Patchett, P.J., 2011, U–Pb–Hf characterization of the central Coast Mountains batholith: Implications for petrogenesis and crustal architecture: *Lithosphere*, v. 3, p. 247–260, <https://doi.org/10.1130/L134.1>.
- Condon, D.J., Schoene, B., McLean, N.M., Bowring, S.A., and Parrish, R.R., 2015, Metrology and traceability of U–Pb isotope dilution geochronology (EARTHTIME Tracer Calibration Part I): *Geochimica et Cosmochimica Acta*, v. 164, p. 464–480, <https://doi.org/10.1016/j.gca.2015.05.026>.
- Creaser, R.A., Price, R.C., and Wormald, R.J., 1991, A-type granites revisited: Assessment of a residual-source model: *Geology*, v. 19, p. 163–166, [https://doi.org/10.1130/0091-7613\(1991\)019<0163:ATGRAO>2.3.CO;2](https://doi.org/10.1130/0091-7613(1991)019<0163:ATGRAO>2.3.CO;2).
- Davis, B.R., and Mosher, S., 2015, Complex structural and fluid flow evolution along the Grenville Front, west Texas: *Geosphere*, v. 11, p. 868–898, <https://doi.org/10.1130/GES01098.1>.
- DeLong, S.E., and Long, L.E., 1976, Petrology and Rb–Sr age of Precambrian rhyolitic dikes, Llano County, Texas: *Geological Society of America Bulletin*, v. 87, p. 275–280, [https://doi.org/10.1130/0016-7606\(1976\)87<275:PARAOP>2.0.CO;2](https://doi.org/10.1130/0016-7606(1976)87<275:PARAOP>2.0.CO;2).
- Dhuime, B., Hawkesworth, C., and Cawood, P., 2011, When continents formed: *Science*, v. 331, p. 154–155, <https://doi.org/10.1126/science.1201245>.
- Ersoy, Y., and Helvacı, C., 2010, FC-AFC-FCA and mixing modeler: A Microsoft® Excel® spreadsheet program for modeling geochemical differentiation of magma by crystal fractionation, crustal assimilation and mixing: *Computers & Geosciences*, v. 36, p. 383–390, <https://doi.org/10.1016/j.cageo.2009.06.007>.
- Ewing, T.E., compiler, 1990, Tectonic map of Texas: University of Texas at Austin, Bureau of Economic Geology State Map SM1, scale 1:750,000, 11 sheets.
- Foland, K.A., and Allen, J.C., 1991, Magma sources for Mesozoic anorogenic granites of the White Mountain magma series, New England, USA: *Contributions to Mineralogy and Petrology*, v. 109, p. 195–211, <https://doi.org/10.1007/BF00306479>.
- Frost, B.R., Barnes, C.G., Collins, W.J., Ellis, D.J., and Frost, C.D., 2001, A geochemical classification for granitic rocks: *Journal of Petrology*, v. 42, p. 2033–2048, <https://doi.org/10.1093/petrology/42.11.2033>.
- Frost, C.D., and Frost, B.R., 2011, On ferroan (A-type) granitoids: Their compositional variability and modes of origin: *Journal of Petrology*, v. 52, p. 39–53, <https://doi.org/10.1093/petrology/egq070>.
- Gardiner, N.J., Hawkesworth, C.J., Robb, L.J., Mulder, J.A., Wainwright, A.N., and Cawood, P.A., 2021, Metal anomalies in zircon as a record of granite-hosted mineralization: *Chemical Geology*, v. 585, <https://doi.org/10.1016/j.chemgeo.2021.120580>.
- Garrison, J.R., Jr., Long, L.E., and Richmann, D.L., 1979, Rb–Sr and K–Ar geochronologic and isotopic studies, Llano Uplift, central Texas: *Contributions to Mineralogy and Petrology*, v. 69, p. 361–374, <https://doi.org/10.1007/BF00372262>.
- Gehrels, G., and Pecha, M., 2014, Detrital zircon U–Pb geochronology and Hf isotope geochemistry of Paleozoic and Triassic passive margin strata of western North America: *Geosphere*, v. 10, p. 49–65, <https://doi.org/10.1130/GES00889.1>.
- Gehrels, G.E., Valencia, V.A., and Ruiz, J., 2008, Enhanced precision, accuracy, efficiency, and spatial resolution of U–Pb ages by laser ablation–multicollector–inductively coupled plasma–mass spectrometry: *Geochemistry Geophysics Geosystems*, v. 9, Q03017, <https://doi.org/10.1029/2007GC001805>.
- Goodge, J.W., and Vervoort, J.D., 2006, Origin of Mesoproterozoic A-type granites in Laurentia: Hf isotope evidence: *Earth and Planetary Science Letters*, v. 243, p. 711–731, <https://doi.org/10.1016/j.epsl.2006.01.040>.
- Grimes, S.W., and Copeland, P., 2004, Thermochronology of the Grenville Orogeny in west Texas: *Precambrian Research*, v. 131, p. 23–54, <https://doi.org/10.1016/j.precamres.2003.12.004>.
- Guitreau, M., Mukasa, S.B., Blichert-Toft, J., and Fahnstock, M.F., 2016, Pikes Peak batholith (Colorado, USA) revisited: A SIMS and LA–ICP–MS study of zircon U–Pb ages combined with solution Hf isotopic compositions: *Precambrian Research*, v. 280, p. 179–194, <https://doi.org/10.1016/j.precamres.2016.05.001>.
- Hammond, J.G., 1990, Middle Proterozoic diabase intrusions in the southwestern U.S.A. as indicators of limited extensional tectonism, *in* Gower, C.F., Rivers, T., and Ryan, B., eds., *Mid-Proterozoic Laurentia-Baltica: Geological Association of Canada Special Paper 38*, p. 517–531.
- Hantsche, A.L., 2015, Hafnium isotope evidence on the source of Grenvillian detrital zircon deposited at the Great Unconformity [M.S. thesis]: Boulder, University of Colorado, 24 p.

- Harbour, R.L., 1960, Precambrian rocks at North Franklin Mountain, Texas: American Association of Petroleum Geologists Bulletin, v. 44, p. 1785–1792, <https://doi.org/10.1306/0BDA6242-16BD-11D7-8645000102C1865D>.
- Harbour, R.L., 1972, Geology of the northern Franklin Mountains, Texas and New Mexico: U.S. Geological Survey Bulletin 1298, 129 p., <https://doi.org/10.3133/b1298>.
- Helper, M.A., 1996, Inks Lake State Park, Valley Spring Gneiss at Spring Creek, in Mosher, S., ed., Guide to the Precambrian Geology of the Eastern Llano Uplift, Central Texas: Field Trip Guide for the Geological Society of America 30th Annual South-Central Section Meeting, Austin, Texas, Spring 1996: Austin, University of Texas at Austin, Department of Geological Sciences, p. 30–31.
- Hollocher, K., Robinson, P., Walsh, E., and Roberts, D., 2012, Geochemistry of amphibolite-facies volcanics and gabbros of the Støren Nappe in extensions west and southwest of Trondheim, Western Gneiss Region, Norway: A key to correlations and paleotectonic settings: American Journal of Science, v. 312, p. 357–416, <https://doi.org/10.2475/04.2012.01>.
- Howard, A.L., 2013, Hafnium isotope evidence on the provenance of ~1.1 Ga detrital zircons from western North America [M.S. thesis]: Boulder, University of Colorado, 107 p.
- Howard, K.A., 1991, Intrusion of horizontal dikes: Tectonic significance of Middle Proterozoic diabase sheets widespread in the upper crust of the southwestern United States: Journal of Geophysical Research, v. 96, p. 12,461–12,478, <https://doi.org/10.1029/91JB00112>.
- Jaffey, A.H., Flynn, K.F., Glendenin, L.E., Bentley, W.C., and Essling, A.M., 1971, Precision measurements of half-lives and specific activities of ^{235}U and ^{238}U : Physical Review C, v. 4, p. 1889–1906.
- Kargi, H., and Barnes, C.G., 1995, A Grenville-age layered intrusion in the subsurface of west Texas: Petrology, petrography, and possible tectonic setting: Canadian Journal of Earth Sciences, v. 32, p. 2159–2166, <https://doi.org/10.1139/e95-168>.
- Keller, G.R., Hills, J.M., Baker, M.R., and Wallin, E.T., 1989, Geophysical and geochronological constraints on the extent and age of mafic intrusions in the basement of west Texas and eastern New Mexico: Geology, v. 11, p. 1049–1052, [https://doi.org/10.1130/0091-7613\(1989\)017<1049:GAGCOT>2.3.CO;2](https://doi.org/10.1130/0091-7613(1989)017<1049:GAGCOT>2.3.CO;2).
- Kelley, V.C., 1968, Geology of the alkaline Precambrian rocks at Pajarito Mountain, Otero County, New Mexico: Geological Society of America Bulletin, v. 79, p. 1565–1572, [https://doi.org/10.1130/0016-7606\(1968\)79\[1565:GOTAPR\]2.0.CO;2](https://doi.org/10.1130/0016-7606(1968)79[1565:GOTAPR]2.0.CO;2).
- Kerr, A., and Fryer, B.J., 1993, Nd isotope evidence for crust-mantle interaction in the generation of A-type granitoid suites in Labrador, Canada: Chemical Geology, v. 104, p. 39–60, [https://doi.org/10.1016/0009-2541\(93\)90141-5](https://doi.org/10.1016/0009-2541(93)90141-5).
- Larson, E.E., Patterson, P.E., and Mutschler, F.E., 1994, Lithology, age, and origin of the Proterozoic Cardenas Basalt, Grand Canyon, Arizona: Precambrian Research, v. 65, p. 255–276, [https://doi.org/10.1016/0301-9268\(94\)90108-2](https://doi.org/10.1016/0301-9268(94)90108-2).
- Li, Y.J., Barnes, M.A., Barnes, C.G., and Frost, C.D., 2007, Grenville-age A-type and related magmatism in southern Laurentia, Texas and New Mexico, U.S.A.: Lithos, v. 97, p. 58–87, <https://doi.org/10.1016/j.lithos.2006.12.010>.
- Ludwig, K.R., 2003, User's manual for Isoplot 3.00: Berkeley, California, Berkeley Geochronology Center, 70 p.
- Manikyamba, C., and Kerrich, R., 2012, Eastern Dharwar Craton, India: Continental lithosphere growth by accretion of diverse plume and arc terranes: Geoscience Frontiers, v. 3, p. 225–240, <https://doi.org/10.1016/j.gsf.2011.11.009>.
- Mattinson, J.M., 2005, Zircon U-Pb chemical abrasion (“CA-TIMS”) method: Combined annealing and multi-step partial dissolution analysis for improved precision and accuracy of zircon ages: Chemical Geology, v. 220, p. 47–66, <https://doi.org/10.1016/j.chemgeo.2005.03.011>.
- McAnulty, W.N., Jr., 1967, Geology of the Fusselman Canyon area, Franklin Mountains, El Paso County, Texas: [unpublished M.S. thesis]: Austin, University of Texas, 79 p.
- McLelland, J., Daly, J.S., and McLelland, J.M., 1996, The Grenville Orogenic Cycle (ca. 1350–1000 Ma): An Adirondack perspective: Tectonophysics, v. 265, p. 1–28, [https://doi.org/10.1016/S0040-1951\(96\)00144-8](https://doi.org/10.1016/S0040-1951(96)00144-8).
- Merdith, A.S., Collins, A.S., Williams, S.E., Pisarevsky, S., Foden, J.D., Archibald, D.B., Blades, M.L., Alessio, B.L., Armistead, S., Plavsa, D., Clark, C., and Müller, R.D., 2017, A full-plate global reconstruction of the Neoproterozoic: Gondwana Research, v. 50, p. 84–134, <https://doi.org/10.1016/j.gr.2017.04.001>.
- Mosher, S., 1993, Western extensions of Grenville age rocks, Texas, in Reed, J.C., Jr., Bickford, M.E., Houston, R.S., Link, P.K., Rankin, D.W., Sims, P.K., and Van Schmus, W.R., eds., Precambrian: Conterminous U.S.: Boulder, Colorado, Geological Society of America, The Geology of North America, v. C-2, p. 366–378.
- Mosher, S., 1998, Tectonic evolution of the southern Laurentian Grenville orogenic belt: Geological Society of America Bulletin, v. 110, p. 1357–1375, [https://doi.org/10.1130/0016-7606\(1998\)110<1357:TEOTSL>2.3.CO;2](https://doi.org/10.1130/0016-7606(1998)110<1357:TEOTSL>2.3.CO;2).
- Mosher, S., Levine, J.S.F., and Carlson, W.D., 2008, Mesoproterozoic plate tectonics: A collisional model for the Grenville-aged orogenic belt in the Llano uplift, central Texas: Geology, v. 36, p. 55–58, <https://doi.org/10.1130/G24049A.1>.
- Mueller, P.A., Kamenov, G.D., Heatherington, A.L., and Richards, J., 2008, Crustal evolution in the southern Appalachian orogen: Evidence from Hf isotopes in detrital zircons: The Journal of Geology, v. 116, p. 414–422, <https://doi.org/10.1086/589311>.
- Mulder, J.A., Karlstrom, K.E., Fletcher, K., Heizler, M.T., Timmons, J.M., Crossey, L.J., Gehrels, G.E., and Pecha, M., 2017, The syn-orogenic sedimentary record of the Grenville Orogeny in southwest Laurentia: Precambrian Research, v. 294, p. 33–52, <https://doi.org/10.1016/j.precamres.2017.03.006>.
- Mulder, J.A., Karlstrom, K.E., Halpin, J.A., Merdith, A.S., Spencer, C.J., Berry, R.F., and McDonald, B., 2018, Rodinian devil in disguise: Correlation of 1.25–1.10 Ga strata between Tasmania and Grand Canyon: Geology, v. 46, p. 991–994, <https://doi.org/10.1130/G45225.1>.
- Nelson, B.K., and DePaolo, D.J., 1985, Rapid production of continental crust 1.7 to 1.9 b.y. ago: Nd isotopic evidence from the basement of the North American midcontinent: Geological Society of America Bulletin, v. 96, p. 746–754, [https://doi.org/10.1130/0016-7606\(1985\)96<746:RPOCCT>2.0.CO;2](https://doi.org/10.1130/0016-7606(1985)96<746:RPOCCT>2.0.CO;2).
- Norman, D.I., Condie, K.C., Smith, R.W., and Thomann, W.F., 1987, Geochemical and Sr and Nd isotopic constraints on the origin of the late Proterozoic volcanics and associated tin-bearing granites from the Franklin Mountains, west Texas: Canadian Journal of Earth Sciences, v. 24, p. 830–839, <https://doi.org/10.1139/e87-081>.
- Nowell, G.M., Kempton, P.D., Noble, S.R., Fitton, J.G., Saunders, A.D., Mahoney, J.J., and Taylor, R.N., 1998, High precision Hf isotope measurements of MORB and OIB by thermal ionisation mass spectrometry: Insights into the depleted mantle: Chemical Geology, v. 149, p. 211–233, [https://doi.org/10.1016/S0009-2541\(98\)00036-9](https://doi.org/10.1016/S0009-2541(98)00036-9).
- Padovani, E.R., and Carter, J.L., 1977, Aspects of the deep crustal evolution beneath south central New Mexico, in Heacock, J.G., Keller, G.V., Oliver, J.E., and Simmons, G., eds., The Earth's Crust: American Geophysical Union Geophysical Monograph 20, p. 19–55, <https://doi.org/10.1029/GM020p0019>.
- Patchett, P.J., and Ruiz, J., 1989, Nd isotopes and the origin of Grenville-age rocks in Texas: Implications for Proterozoic evolution of the United States mid-continent region: The Journal of Geology, v. 97, p. 685–695, <https://doi.org/10.1086/629352>.
- Pearce, J.A., 2008, Geochemical fingerprinting of oceanic basalts with applications to ophiolite classification and the search for Archean oceanic crust: Lithos, v. 100, p. 14–48, <https://doi.org/10.1016/j.lithos.2007.06.016>.
- Pittenger, M.A., Marsaglia, K.M., and Bickford, M.E., 1994, Depositional history of the middle Proterozoic Cadstner Marble and basal Mundy Breccia, Franklin Mountains, West Texas: Journal of Sedimentary Research, v. 64, p. 282–297, <https://doi.org/10.1306/D4267FAF-2B26-11D7-8648000102C1865D>.
- Roback, R.C., 1996, Characterization and tectonic evolution of a Mesoproterozoic island arc in the southern Grenville Orogen, Llano uplift, central Texas: Tectonophysics, v. 265, p. 29–52, [https://doi.org/10.1016/S0040-1951\(96\)00145-X](https://doi.org/10.1016/S0040-1951(96)00145-X).
- Roths, P.J., 1993, Geochemical and geochronological studies of the Grenville-age (1200–1000 Ma) Allamoore and Hazel Formations, Hudspeth and Culberson Counties, west Texas, in Soegaard, K., Nielsen, K.C., Marsaglia, K.M., and Barnes, C.G., eds., Precambrian Geology of the Franklin Mountains and Van Horn Area, Trans-Pecos Texas: Dallas, Texas, Geological Society of America, South-Central Section, University of Texas, p. 11–35.
- Rougvie, J.R., Carlson, W.D., Copeland, P., and Connelly, J.N., Roback, R.C., and Copeland, P., 1999, Late thermal evolution of Proterozoic rocks in the northeastern Llano uplift, central Texas: Precambrian Research, v. 94, p. 49–72, [https://doi.org/10.1016/1093-S0301-9268\(98\)00103-X](https://doi.org/10.1016/1093-S0301-9268(98)00103-X).
- Rudnick, R.L., 1983, Geochemistry and tectonic affinities of a Proterozoic bimodal igneous suite, west Texas: Geology, v. 11, p. 352–355, [https://doi.org/10.1130/0091-7613\(1983\)11<352:GATAOA>2.0.CO;2](https://doi.org/10.1130/0091-7613(1983)11<352:GATAOA>2.0.CO;2).
- Rudnick, R.L., and Gao, S., 2003, Composition of the continental crust, in Rudnick, R.L., ed., Treatise on Geochemistry, Volume 3: The Crust: Oxford, UK, Elsevier, p. 1–64, <https://doi.org/10.1016/B0-08-043751-6/03016-4>.
- Seeley, J.M., 1999, Studies of the Proterozoic tectonic evolution of the southwestern United States [Ph.D. thesis]: El Paso, University of Texas, 321 p.

- Shannon, W.M., Barnes, C.G., and Bickford, M.E., 1997, Grenville magmatism in west Texas: Petrology and geochemistry of the Red Bluff granitic suite: *Journal of Petrology*, v. 38, p. 1279–1305, <https://doi.org/10.1093/ptro/38.10.1279>.
- Smith, D.R., Barnes, C., Shannon, W., Roback, R., and James, E., 1997, Petrogenesis of Mid-Proterozoic granitic magma: Examples from central and west Texas: *Precambrian Research*, v. 85, p. 53–79, [https://doi.org/10.1016/S0301-9268\(97\)00032-6](https://doi.org/10.1016/S0301-9268(97)00032-6).
- Smith, D.R., Noblett, J., Wobus, R.A., Unruh, D., Douglass, J., Beane, R., Davis, C., Goldman, S., Kay, G., Gustavson, B., Saltoun, B., and Stewart, J., 1999, Petrology and geochemistry of late-stage intrusions of the A-type, mid-Proterozoic Pikes Peak batholith (Central Colorado, USA): Implications for petrogenetic models: *Precambrian Research*, v. 98, p. 271–305, [https://doi.org/10.1016/S0301-9268\(99\)00049-2](https://doi.org/10.1016/S0301-9268(99)00049-2).
- Soegaard, K., and Callahan, D.M., 1994, Late Middle Proterozoic Hazel Formation near Van Horn, Trans-Pecos Texas: Evidence for transpressive deformation in Grenvillian basement: *Geological Society of America Bulletin*, v. 106, p. 413–423, [https://doi.org/10.1130/0016-7606\(1994\)106<0413:LMPHFN>2.3.CO;2](https://doi.org/10.1130/0016-7606(1994)106<0413:LMPHFN>2.3.CO;2).
- Spencer, C.J., Prave, A.R., Cawood, P.A., and Roberts, N.M.W., 2014, Detrital zircon geochronology of the Grenville/Llano foreland and basal Sauk Sequence in west Texas, USA: *Geological Society of America Bulletin*, v. 126, p. 1117–1128, <https://doi.org/10.1130/B30884.1>.
- Spencer, C.J., Kirkland, C.L., Roberts, N.M.W., Evans, N.J., and Liebmann, J., 2020, Strategies towards robust interpretations of in situ zircon Lu-Hf isotope analyses: *Geoscience Frontiers*, v. 11, p. 843–853, <https://doi.org/10.1016/j.gsf.2019.09.004>.
- Streckeisen, A.L., and LeMaitre, R.W., 1979, A chemical approximation to the modal QAPF classification of the igneous rocks: *Neues Jahrbuch für Mineralogie, Abhandlungen*, v. 136, p. 169–206.
- Taylor, S.R., and McLennan, S.M., 1995, The geochemical evolution of the continental crust: *Reviews of Geophysics*, v. 33, p. 241–265, <https://doi.org/10.1029/95RG00262>.
- Thomann, W.F., and Hoffer, R.L., 1991, Progressive contact metamorphism of Middle Proterozoic Castner Marble, Franklin Mountains, Texas: *Contributions to Geology, University of Wyoming*, v. 29, p. 71–80.
- Timmons, J.M., Karlstrom, K.E., Heizler, M.T., Bowring, S.A., Gehrels, G.E., and Crossey, L.J., 2005, Tectonic inferences from the ca. 1255–1100 Ma Unkar Group and Nankowep Formation, Grand Canyon: Intracratonic deformation and basin formation during protracted Grenville-age orogenesis: *Geological Society of America Bulletin*, v. 117, p. 1573–1595, <https://doi.org/10.1130/B25538.1>.
- Turner, S.P., Foden, J.D., and Morrison, R.S., 1992, Derivation of some A-type magmas by fractionation of basaltic magma: An example from the Padthaway Ridge, South Australia: *Lithos*, v. 28, p. 151–179, [https://doi.org/10.1016/0024-4937\(92\)90029-X](https://doi.org/10.1016/0024-4937(92)90029-X).
- Van Schmus, W.R., Bickford, M.E., and Turek, A., 1996, Proterozoic geology of the east-central Midcontinent basement, in van der Pluijm, B.A., and Catacosinos, P.A., eds., *Basement and Basins of Eastern North America: Geological Society of America Special Paper 308*, p. 7–32, <https://doi.org/10.1130/0-8137-2308-6.7>.
- Vervoort, J.D., and Blichert-Toft, J., 1999, Evolution of the depleted mantle: Hf isotope evidence from juvenile rocks through time: *Geochimica et Cosmochimica Acta*, v. 63, p. 533–556, [https://doi.org/10.1016/S0016-7037\(98\)00274-9](https://doi.org/10.1016/S0016-7037(98)00274-9).
- Vervoort, J.D., and Kemp, A.I., 2016, Clarifying the zircon Hf isotope record of crust-mantle evolution: *Chemical Geology*, v. 425, p. 65–75, <https://doi.org/10.1016/j.chemgeo.2016.01.023>.
- Vonopartis, L., Nex, P., Kinnaird, J., and Robb, L., 2020, Evaluating the changes from endogranitic magmatic to magmatic-hydrothermal mineralization: The Zaaiploaats tin granites, Bushveld Igneous Complex, South Africa: *Minerals (Basel)*, v. 10, no. 4, 379, <https://doi.org/10.3390/min10040379>.
- Walker, N.W., 1992, Middle Proterozoic geologic evolution of the Llano uplift, Texas: Evidence from U-Pb zircon geochronometry: *Geological Society of America Bulletin*, v. 104, p. 494–504, [https://doi.org/10.1130/0016-7606\(1992\)104<0494:MPGEO>2.3.CO;2](https://doi.org/10.1130/0016-7606(1992)104<0494:MPGEO>2.3.CO;2).
- Whalen, J.B., and Frost, C.D., 2013, The Q-ANOR diagram: A tool for the petrogenetic and tectonomagmatic characterization of granitic suites: *Geological Society of America Abstracts with Programs*, v. 45, no. 3, p. 24.
- Whalen, J.B., and Hildebrand, R.S., 2019, Trace element discrimination of arc, slab failure, and A-type granitic rocks: *Lithos*, v. 348–349, <https://doi.org/10.1016/j.lithos.2019.105179>.
- Wooden, J.L., Barth, A.P., and Mueller, P.A., 2013, Crustal growth and tectonic evolution of the Mojave crustal province: insights from hafnium isotope systematics in zircons: *Lithosphere*, v. 5, p. 17–28, <https://doi.org/10.1130/L218.1>.
- Wrucke, C.T., 1989, The middle Proterozoic Apache Group, Troy Quartzite, and associated diabase of Arizona, in Jenney, J.P., and Reynolds, S.J., eds., *Geologic Evolution of Arizona: Arizona Geological Society Digest 17*, p. 239–258.
- Zartman, R.E., 1964, A geochronologic study of the Lone Grove pluton from the Llano Uplift, Texas: *Journal of Petrology*, v. 5, p. 359–409, <https://doi.org/10.1093/ptrology/5.3.359>.
- Zartman, R.E., 1965, The isotopic composition of lead in microclines from the Llano uplift, Texas: *Journal of Geophysical Research*, v. 70, p. 965–975, <https://doi.org/10.1029/JZ070i004p00965>.